Model Estimate of Pan-Arctic Wetland Methane Emissions and Their Climate Sensitivity during 1960-2006

Xiaodong Chen

A thesis

submitted in partial fulfillment of the

requirements for the degree of

Master of Science in Civil Engineering

University of Washington

2015

Committee:

Dennis P. Lettenmaier

Bart Nijssen

Rebecca B. Neumann

Theodore J. Bohn

Program Authorized to Offer Degree:

Department of Civil and Environmental Engineering

University of Washington

Abstract

Model Estimate of Pan-Arctic Wetland Methane Emissions and Their Climate Sensitivity during 1960-2006

Xiaodong Chen

Chair of the Supervisory Committee:

Professor Dennis P. Lettenmaier

Department of Civil and Environmental Engineering

We employed a linked hydro-biogeochemical model framework to study the surface methane emissions from Pan-Arctic wetlands over the period 1948-2006. We also performed a set of climate control experiments to investigate the sensitivity of methane emissions to climate change over 1960-2006. We estimated the average methane emission from Pan-Arctic wetlands during 1960-2006 as 35.05 ± 6.66 $TgCH_4$/year. This is slightly higher than the previous studies. The wetland methane emissions showed a significant increasing trend of 0.15$TgCH_4$/year ($p<10^{-5}$). Changes in air temperature are the cause of most of the inferred trend. At 5% significance level, over 90% of the increase in the wetland methane emissions during 1960-2006 can be attributed to climate warming. We also found that the climate sensitivity of CH_4 emissions is relatively constant at the grid scale. Based on these inferred coefficients, we estimate that the Pan-Arctic wetland methane emissions will continue to increase under RCP4.5 climate scenario, and the 2100s emission would be 135% of the 2000s level.

ACKNOWLEDGEMENTS

First, I would like to express my gratitude and appreciation to my supervisor Dr. Dennis Lettenmaier for his great help during my master study. He introduced me to this field and showed me how to work as a professional and passionate researcher. I am also thankful for the support of Dr. Bart Nijssen and Dr. Rebecca Neumann as my committee members.

Also, I would like to sincerely thank Dr. Theodore Bohn, for his long-time help in developing modelling framework for this study. He has shown me what it means to be a responsible and careful researcher.

At last I am grateful to my family, for their comprehension and support to my study.

Table of Contents

List of Figures

List of Tables

1. Introduction

1.1 Background and motivation

Methane is an important greenhouse gas, which although having concentrations only about 0.5% of CO_2, has a per unit mass greenhouse warming potential that is about 25 times larger. Various studies have shown that wetlands are the largest natural methane source (Fung et al., 1991; Hein, Crutzen, & Heimann, 1997; Solomon, 2007) globally. According to the Global Lakes and Wetlands data base of Lehner and Döll (2004), the northern high latitudes contain about one-half of the world's wetlands. These wetlands are experiencing more rapid climate change than elsewhere globally (Diffenbaugh & Giorgi, 2012; Serreze et al., 2000), thus giving rise to concerns as to their increasing role in global methane emissions.

Over the past few decades, attempts have been made to estimate the distribution of surface methane emissions from high latitude wetlands. These attempts have been based on in situ observations (Crill et al., 1988; Glagolev, Kleptsova, Filippov, Maksyutov, & Machida, 2011; Levy et al., 2012; Matthews & Fung, 1987; Sebacher, Harriss, Bartlett, Sebacher, & Grice, 1986), inverse atmospheric modelling (Bousquet et al., 2006; Chen & Prinn, 2006; Hein et al., 1997; Houweling, Kaminski, Dentener, Lelieveld, & Heimann, 1999; Meirink, Bergamaschi, & Krol, 2008), or process-based hydro-ecological models (Cao, Marshall, & Gregson, 1996; Walter & Heimann, 2000; Zhu, Zhuang, Lu, & Song, 2014).

Methane emission rates in wetlands depend on a number of environmental and climate

controls. For instance, Christensen et al. (2003) investigated the role of soil temperature and soil carbon input, and concluded that almost all of the variation in annual wetland methane emissions can be attributed to variations in soil temperature and substrate content (i.e. the mineral and organic content in the soil). Saarnio et al. (1997), Walter and Heimann (2001) investigated the relationship between methane emissions and soil moisture availability, and found methane emission rate is negatively correlated with ground water table depth. Sabrekov et al. (2014) found that water table depth dominated the variance in methane emissions at daily time scales at a few bogs in Siberia. Bohn and Lettenmaier (2010) confirmed the importance of soil moisture heterogeneity within wetlands at the sub grid scale and annual scale. Methane emissions also depend on carbon substrate availability, which itself is a function of plant productivity (Walter and Heimann, 2000), as well as other factors such as pH, oxidation state and the nitrogen cycle (Spahni et al., 2011; Zhuang et al., 2004). Many of these environmental factors interact and compete. For example, Bohn et al. (2007) showed that air temperature and precipitation exert competing influences over the water table position, through winter snow accumulation, spring snow melt, and summer evapotranspiration; and over metabolic rates; leading to trade-offs in their influences over emissions.

The complex interactions between the many factors controlling methane emissions can obscure our understanding of their behavior. Some insights may be gained by identifying the conditions under which a single limiting factor dominates the behavior of emissions. Nemani et al. (2003) found that NPP is limited by temperature and radiation at high latitudes,

but water at lower latitudes. Teuling et al. (2009) and Sineveratne et al (2010) investigated global climate controls on annual evapotranspiration (ET), and found that temperature is the dominant control over northern Eurasia, while precipitation is a key control at mid-low latitudes and in northern Canada. Taken together, these studies established a framework of climate control analysis that can be applied to wetland methane emissions over large areas.

Previous studies have explored the response of methane to historical or projected future changes in climate. For example, Chen and Prinn (2006) evaluated wetland methane emissions during a five-year period 1996-2001 from global wetlands and rice paddies. Zhu et al (2014) constructed a high resolution map of methane emissions for the entire Pan-Arctic domain, but the simulation was only performed for 1993-2004. Some other studies (Riley et al., 2011; Ringeval et al., 2010; Spahni et al., 2011) also estimated methane emissions at large scales, but most only produce results over the most recent two decades or so. On the other hand, some studies evaluating historical long-term methane emissions have been performed over smaller spatial domains. Bohn et al (2013), for instance, investigated hydro-carbon conditions in wetlands, but their study is limited to the West Siberia Lowland (WSL). Future projections have been performed at large scale by Zhu et al. (2011) and Gedney et al. (2004), which predicted 6-51% increase from the northern Eurasia and near-doubling from global wetland by 2100, respectively. However, these studies did not investigate which climate factors were the dominant drivers of CH_4 emissions, or how they vary in space and time.

1.2 Science questions for this study

We focus here on the spatial variability of methane emissions and trends therein over the northern Pan-Arctic wetlands over the last half century. We address three questions:

(1) What have been the aggregate long-term methane emissions from the Pan-Arctic wetland area over the last half century, and how has it changed?

(2) What have been the dominant factor(s) that have controlled changes in the space- time variability of methane emissions over that time period?

(3) How will these conditions be affected by a changing climate?

In answering question (2) and (3), we develop sensitivity maps for Pan-Arctic wetland methane emissions. These sensitivity maps provide us with a basis for projecting future emissions in the region.

1.3 Thesis outline

Chapter 2 presents the modelling framework and the dataset employed for this study, as well as the experiment design. Chapter 3 shows the results from this study, and it is composed of historical simulation results and sensitivity experiments results. It is followed by a short discussion in Chapter 4.

2. Study methods

2.1 Study Domain

Our study domain is the Pan-Arctic land area, which we define as the global land area north of about 45°N (Figure 2.1a). The domain boundaries are as in the TransCom project (Gurney, Law, Rayner, & Denning, 2000), except that we exclude Greenland. We also include southern Russia and the permafrost part of Tibet, so the domain covers essentially the entire northern hemisphere permafrost land area, aside from a few high altitude areas.

This domain includes three major wetland areas: the West Siberia Lowland (WSL), the Scandinavia region, and the Hudson's Bay Lowland (HBL). There are also many smaller wetlands distributed over the domain. Forests cover about 23% of the total land area of the study domain, as evidenced by the belt of high values of leaf area index (LAI) between about 55˚ and 65˚N (Figure 2.1b).

The region contains many peatlands, which are reservoirs of organic carbon (Tarnocai et al., 2009), and have the potential to produce huge fluxes of carbon (CO_2 or CH_4) to the atmosphere. Most of the northern hemisphere permafrost (Figure 2.1c) also lies within this area. Within the permafrost areas, deep soil temperatures are generally below 0°C for successive years, which restricts biological methanogens. However, during summer, the active layer (seasonally thawed) provides a suitable environment for bio-methane production.

Our simulation period is 1948-2006. We first ran the model for 50 years to stabilize its moisture and carbon storages. Then starting from the soil states at the end of this 50- year run, we performed simulations for 1960-2006. To isolate the effects of various climate factors

that drive the variability in CH_4 emissions, we performed five control experiments in which we held one of four variables (air temperature, precipitation, atmospheric CO_2 concentration, and solar radiation) constant during 1960-2006.

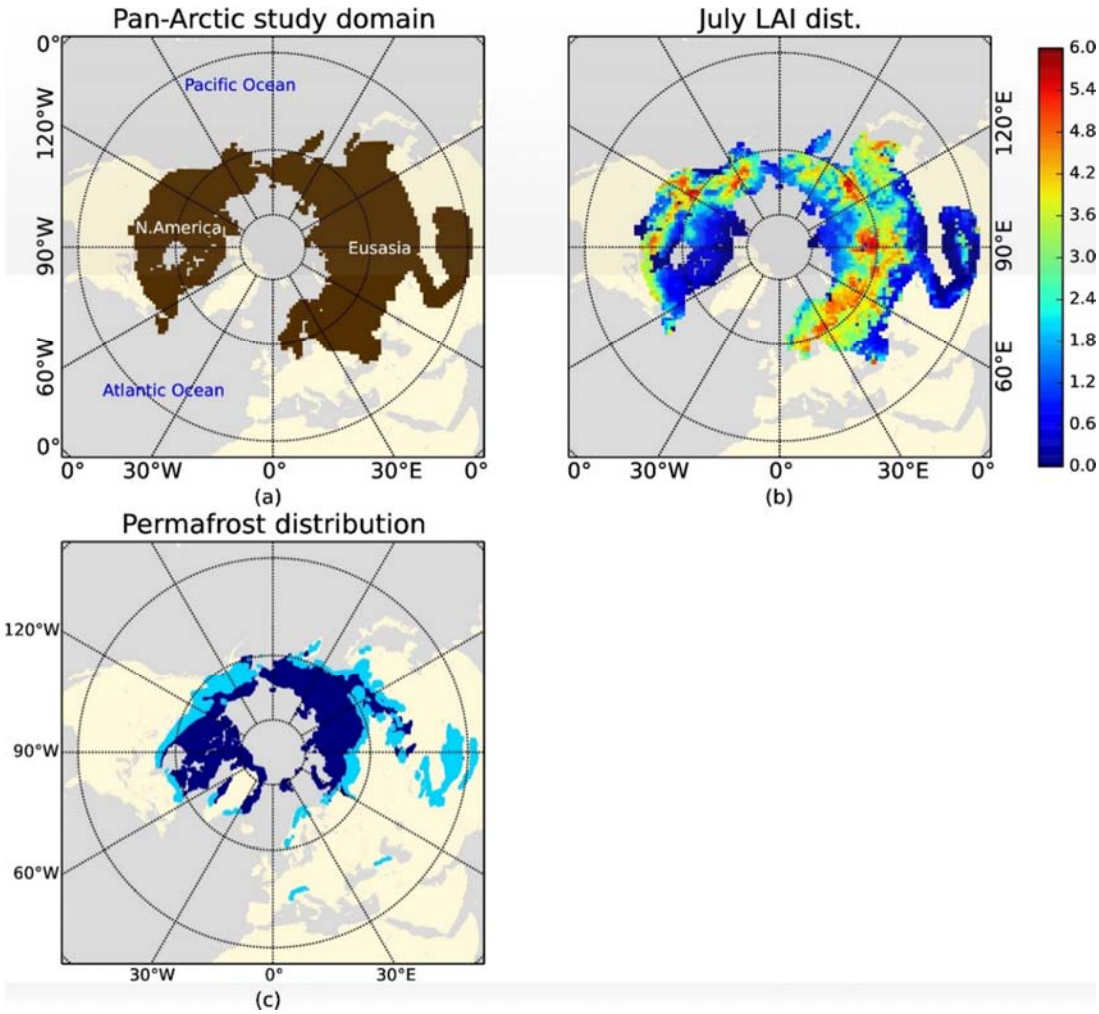

Figure 2.1: Study domain.

(a) spatial extent of the domain; (b) July LAI (from MODIS MCD15A2 dataset, LP DAAC); (c) permafrost distribution from Circum-Arctic Map of Permafrost and Ground-Ice Conditions (GGD318 database, Brown et al. 2014).

2.2 Model framework

We used a modified version of the Variable Infiltration Capacity (VIC) version 4.1.2 that simulates methane emissions as well as the hydrologic processes represented in the standard version of the VIC model. VIC model resolves the soil moisture and temperature profile through coupled water-energy balance equation, and the permafrost distribution could be derived by computing the soil depth above which soil temperature is below ºC. We provide here a brief description of the model features related to wetland process. The main enhancement of the version of VIC we used is a module for calculating the carbon inputs into the ecosystem, which is the substrate source of biogeochemical processes that produce methane. The model performs a coupled water- energy balance calculation for each grid cell. Within each grid cell the model represents multiple elevation bands (in regions where there are substantial topographic variations within the grid cell) and vegetation classes (the latter as "tiles", as in many LSMs). This modified version of VIC also represents lakes and wetlands as described in Bohn et al. (2013). Each grid cell in the study domain is assumed to be composed of a lake-wetland part and a dry part, with the fraction of lake-wetland and dry parts pre-determined from the MODIS plant functional type dataset MCD12Q1 (http://webmap.ornl.gov/wcsdown/dataset.jsp?ds_id=10004), soil organic carbon content database (Tarnocai et al., 2009) and the Global Lakes and Wetlands data set (GLWD) of Lehner and Doll (2004). Each grid cell is composed of 0.005 degree pixels, and we identify a pixel as wetland if: 1) It is classified as inland water in the MODIS plant functional type map (MCD12Q1), or 2) its soil organic carbon content in the Tarnocai et al. (2009) database is greater than 70%, or 3) it is identified as lake or wetland in the GLWD database. The wetland fractions are shown in Figure 2.2. Figure 2.2 also shows the distribution of seasonally inundated area, and seasonally saturated area together with the location of

permanent lakes. Here inundated areas are those with water levels above the ground surface, while saturated areas have water levels at the surface. In VIC model, NPP reaches a maximum value when inundation fraction within a grid is moderate. More or less inundation will result in reduced NPP. We applied our lake-wetland continuum representation to the lake and wetland part of the domain, which for each grid cell consists of a "composite" lake (single "lake" that has the total area of all lakes in the grid cell, and a depth distribution that follows a parabolic depth-area relationship), and is surrounded by saturated wetlands. The lake bathymetry and land topography within each grid cell are derived from the GTOPO30 digital topographic data (https://lta.cr.usgs.gov/GTOPO30). More details of the lake- wetland continuum are described in Bohn et al (2013).

Using the above classification, we divided the study domain into 3775 100 km EASE grid cells, of which 2040 include wetlands.

The VIC model is linked to the Walter and Heimann methane model (Walter & Heimann, 2000) for methane emissions, which are simulated as in Walter et al. (2001) and Bohn et al. (2007). The Walter and Heimann methane model takes the water table depth distribution, soil temperature profile and net primary productivity (NPP) generated by VIC to calculate the corresponding methane generation rates. The model assumes that some small amount of carbon from NPP leaks into the soil through plant roots, and is converted to CH_4 through anaerobic respiration of methanogen, which depends on the soil thermal and moisture condition.

Calibration of the combined VIC and methane models was performed over West Siberia by Bohn et al. (2013), and we adopted the parameters from that study as given in Table 1. In Bohn et al. (2013), two parameter sets were optimized for the West Siberia lowlands: "south"

(primarily within the forest belt, or taiga) and “north” (primarily tundra). To extend these parameter values across the pan-Arctic domain, we assigned the “south” parameter set to grid cells with July LAI higher than 4, and the “north” parameter set to all other grid cells.

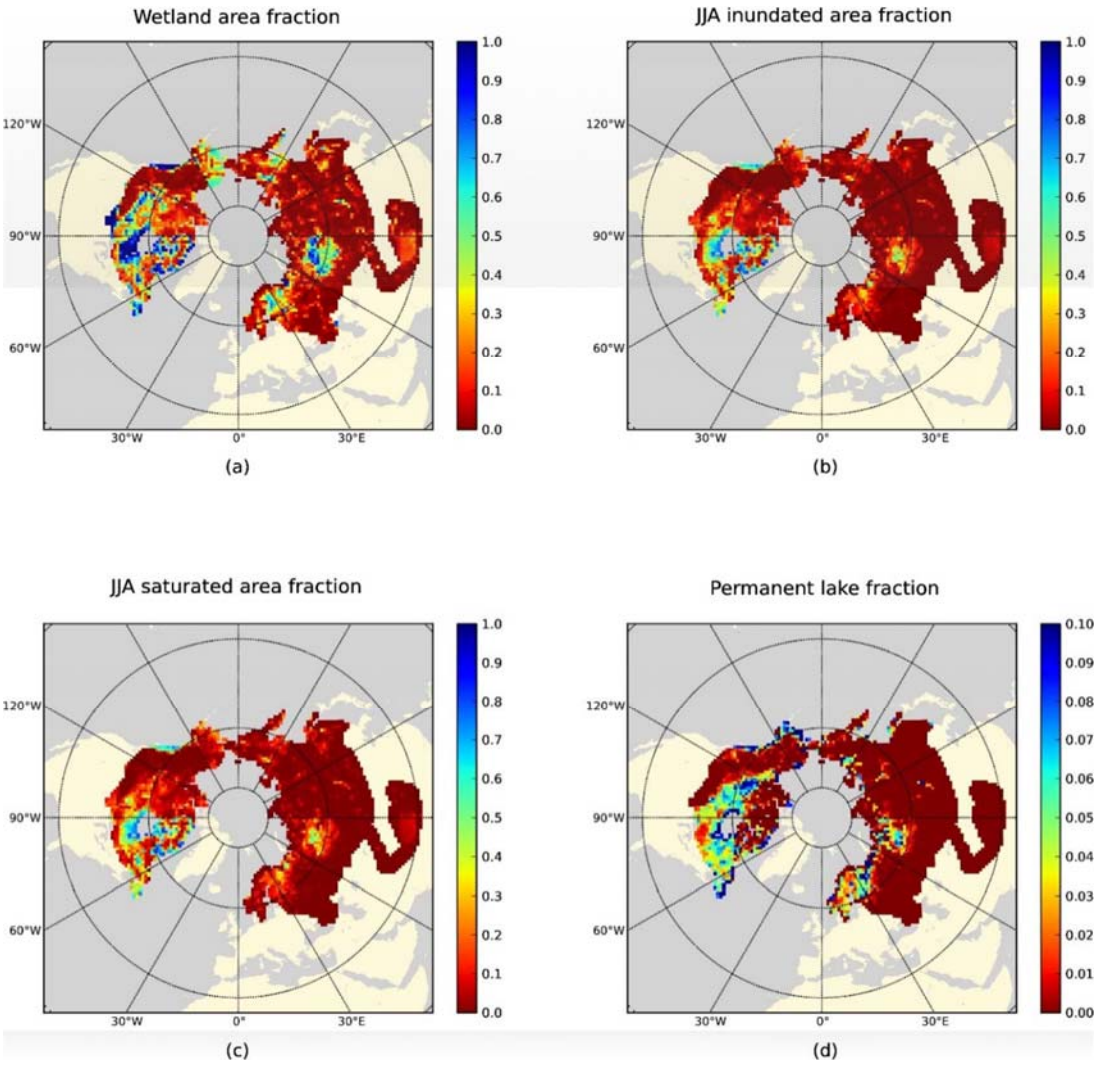

Figure 2.2: Wetland characteristics in the study domain.

(a) fraction of wetland within each grid cell prescribed from GLWD, MODIS land cover, and soil carbon database; (b) fraction of seasonally inundated area during summer (June-August) within each grid cell; (c)

fraction of seasonally saturated area (JJA) within each grid cell; (d) permanent lake distribution in the study domain, shown as fraction of grid cell area. Subplots (b)-(d) are from VIC model runs.

The primary meteorological forcings used to drive the VIC hydrological model include 3-hourly precipitation, air temperature, wind speed, downward shortwave and longwave radiation. These data were obtained from Sheffield et al. (2006) at 0.25x0.25 degree spatial resolution, which we regridded to 100 km EASE-grid. Atmospheric CO_2 concentration data were taken from Bohn et al. (2013).

LAI data were taken from the MODIS MCD15A2 data set for the period 2003-2010. We used the mean seasonal cycle for this period repetitively for every year in our simulation period. Soil parameters were taken from Su et al. (2006).

For the methane oxidation process in the upland part of each grid cell, we assigned an average oxidation rate (Dutaur & Verchot, 2007) to the non-wetland area. This rate is 7.23 x 10^{-5} $gCH_4/m^2/day$ in the boreal forest, and 4.08 x 10^{-5} $gCH_4/m^2/day$ in the tundra area.

Table 1: Parameters used in the Walter and Heimann (2000) methane model

Type	r_0 [(gC m^{-2} $d^{-1}]^{-1}$]	xvmax [µmol L^{-1} h^{-1}]	Rkm [µmol L^{-1}]	rq_{10} [-]	oxq_{10} [-]
North	0.024	0.005	14.635	3.863	5.006
South	0.017	0.272	14.759	10.715	1.683

Note: r0 is reference methane production rate that is related to absolute substrate availability and quality; xvmax is maximum methane oxidation rate; Rkm is the Michaelis Menten constant; rq10 is Q10 value for ethane production rate; oxq10 is Q10 value for methane oxidation rate.

2.3 Sensitivity experiment design

We designed sensitivity experiments to find the relative contribution of each climate factor to methane emissions. We focused on what we found out to be the three most important ones: Air temperature, precipitation and atmospheric CO_2.

We analyzed all five of the meteorological forcing variables for trends at each grid cell. Trends in the forcing variables were removed in cases when the trend was significant at the 0.05 level. Linear trends in air temperature were estimated by linearly regressing the annual mean temperature over time, then cumulative changes since 1960 can be calculated for each year. Trends in downward longwave radiation were handled in a similar way. Trends in annual total precipitation were obtained using linear regression. Then the ratio of detrended annual mean precipitation to annual precipitation in each year was calculated and applied to each day within the year. Trends in downward shortwave radiation were handled similarly to precipitation. These calculations were performed separately for each grid cell. At the 0.05 significance level, the domain as a total shows increasing trends in air temperature, precipitation and downward longwave radiation, but decreasing trend in downward shortwave radiation. For detrended atmospheric CO_2, the concentration level of 1960 was applied to the entire period 1960-2006. Table 2 shows the statistics of the climate forcings in each experiment.

Using these historical and detrended forcings, we designed six experiments to investigate the impact of historical climate change on the wetland methane emissions:

(1) R01: Historical simulation, driven by historical forcings;

(2) R02: Air temperature and longwave radiation (TLW) control run, driven by detrended air temperature and longwave radiation;

(3) R03: CO_2 control run, driven by 1960 CO_2 level;

(4) R04: TLW and precipitation (TLWP) control run, driven by detrended air temperature, detrended longwave radiation, detrended precipitation;

(5) R05: Precipitation (P) control run, driven by detrended precipitation;

(6) R06: Shortwave radiation (SW) control run, driven by detrended shortwave radiation.

Table 2 : Statistics of climate forcing for each run

Run ID	T_{2006} (K)	P_{2006} (mm/year)	$[C02]_{2006}$ (ppm)	LW_{2006} (W/m^2)	SW_{2006} (W/m^2)
R01	269.7	450	381.4	262.9	119.3
R02	268.0	450	381.4	259.1	119.3
R03	269.7	450	316.5	262.9	119.3
R04	268.0	440	381.4	259.1	119.3
R05	269.7	440	381.4	262.9	119.3
R06	269.7	450	381.4	262.9	120.3

2.4 Identifying the dominant emission controls

Dominant emission controls should be highly correlated with emissions over long durations. We calculated the correlation coefficients between CH_4 emissions series and drivers

at grid cell scale, so for each grid cell we have several correlation coefficients.

We determined through the sensitivity experiments which have the largest contribution to the historical changes in CH_4 emissions, and then focused on these drivers. We investigate below the spatial distribution of these coefficients, and through these maps we determine which area is determined by what driver. Together with the average summer T and P of each grid cell, these correlations can also be marked on a T-P space to help understand how they vary under different climate conditions. This should reveal more general characteristics for wetland methane emission under varying climate.

2.5 Future projections

Changes in environmental factors are generally small relative to their mean values, which suggests expressing sensitivity (α) coefficients as:

$$\begin{aligned}
\alpha_p &= \frac{dCH_4}{dP} \quad (\mathrm{gCH_4 \cdot m^{-2} \cdot year^{-1} \cdot mm^{-1}}) \\
\alpha_{TLW} &= \frac{dCH_4}{dT_{air}} \quad (\mathrm{gCH_4 \cdot m^{-2} \cdot year^{-1} \cdot K^{-1}}) \\
\alpha_{CO2} &= \frac{dCH_4}{d[CO_2]} \quad (\mathrm{gCH_4 \cdot m^{-2} \cdot year^{-1} \cdot ppm^{-1}}) \\
\alpha_{SW} &= \frac{dCH_4}{dSW} \quad (\mathrm{gCH_4 \cdot m^{-2} \cdot year^{-1} \cdot (W/m^2)^{-1}})
\end{aligned} \qquad [1]$$

Where the total change in methane emissions due to climate change $\Delta CH_4 = a_P x\ d + a_{TLW} x\ d_{air} + a_{CO} x\ dC0 + a_{SW} x\ dSW + interaction$. These sensitivity coefficients

can be estimated from our climate control experiments.

For each grid cell, we can calculate these four sensitivity coefficients, together with grid cell's average T and P. We can plot these sensitivities in T-P space, as shown in Figure 2.3. The resulting sensitivity map will not only help us understand the wetland characteristics in the study domain, but will also be useful in making future projections. Based on the sensitivity maps for major drivers in T-P space, and given a reference climate condition and corresponding CH_4 emission rate, we can derive the projected emission rate through equation [2].

$$CH_4' = CH_4 + \alpha_P \times dP + \alpha_{TLW} \times dT_{air} + \alpha_{CO2} \times dCO_2 \quad [2]$$

In which CH_4 is the reference methane emission rate, CH_4' is the projected future methane emission rate, other coefficients are as defined in equation [1].

As shown in Figure 2.3, these sensitivities vary under different climate conditions. Given that the CCSM4 future climate will differ from the current (baseline), we will use variable sensitivities corresponding to the future climate instead of fixed sensitivities to make the projections. The value for each grid cell in Figure 2.3 is calculated for the model grid cells whose average historical condition during 1960-2006 fall into that grid cell's climate condition, thus yielding effective sensitivities under climate conditions around this grid. When applying equation [2], we first calculated the decadal average climate conditions (JJA T and JJA P) for each year, then took the corresponding sensitivities from these matrices. These sensitivity coefficients were used in equation [2] for this decade. For example, for year i between 2031 and 2040, the sensitivities were determined by the 2031-2040 average JJA T and JJA P, but forcings in equation [2] were specific to year i.

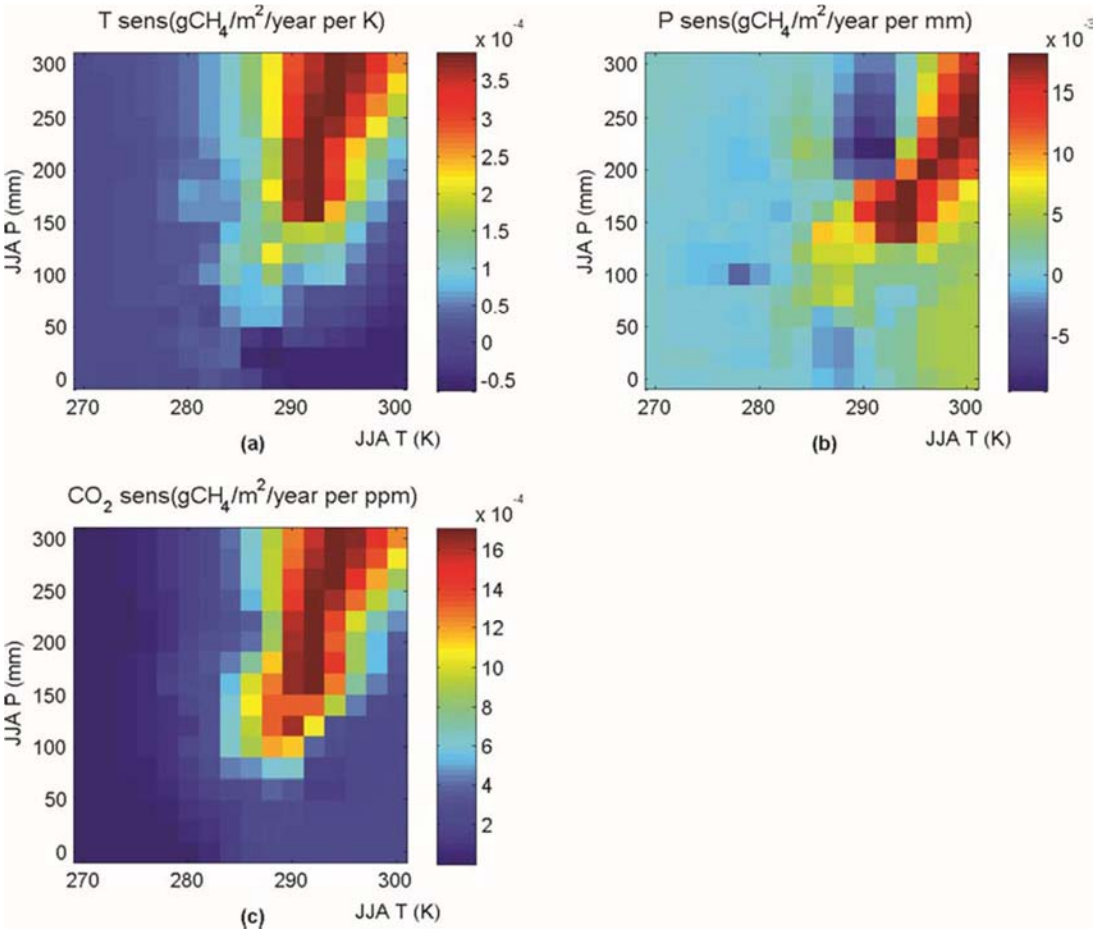

Figure 2.3: 1960-2006 average T, P and CO_2 sensitivities of CH_4 emission in JJA T and JJA P space.

3. Results

3.1 Historical simulation and model validation

We compared the simulated NPP distribution with the MODIS MOD17A3 product (Zhao, Heinsch, Nemani, & Running, 2005). Figure 3.1 shows that model results and MODIS patterns match reasonably well, with high NPP in both model and MODIS for mid-high latitude forested areas in Eurasia and the south of the HBL. The MOD17A3 NPP product is derived from the MODIS land cover and FPAR/LAI database, driven by NCEP/NCAR reanalysis meteorological data. For each of our 3774 grid cells, we computed the 2001-2006 averaged annual NPP for VIC results and MODIS estimates. Then a linear regression of VIC-simulated NPP on MODIS NPP over the study domain (3774 pairs) yields a correlation coefficient of R=0.87. Although wetlands generally have lower LAI than forests, the wetlands in the high-LAI area between 55˚ and 65˚ N latitude band also have higher LAI than their counterparts in the south, due to some forests being interspersed with wetlands. Thus the carbon inputs to these wetlands tend to be higher. This high correlation indicates that the model produces realistic spatial patterns of carbon sources to biological processes.

Reconstruction of the permafrost distribution requires not only the correct simulation of the spatial distribution of soil temperature, but also its temporal evolution. In Figure 3.2, we compare the VIC-simulated active layer depth (ALD) in the permafrost area with the Circum-Arctic Permafrost and Ground-ice condition map (Brown, Ferrians, Heginbottom, & Melnikov, 1997). Panel (a) shows the distribution of continuous and discontinuous permafrost, using the convention that to be classified as permafrost at least half of a grid cell must be so classified. There is a good match between panels (a) and (b), and also the general trend of

smaller ALD corresponding to greater permafrost extent is clear. Examination of the figure suggests that ALD of 1m is an approximate threshold for “continuous permafrost” in the GGD318 dataset.

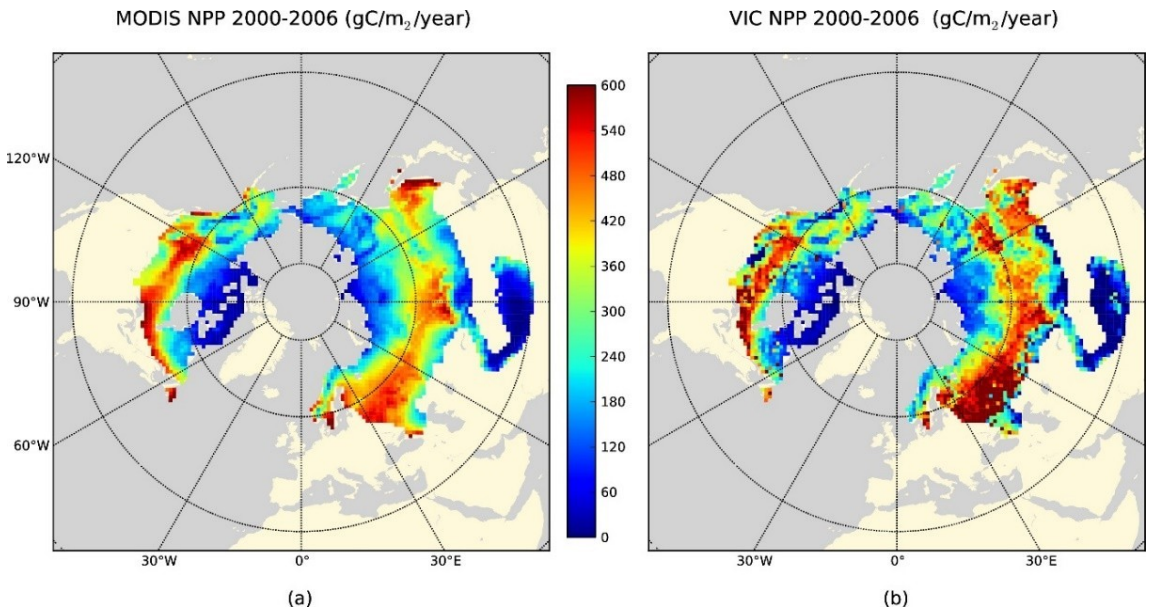

Figure 3.1: Annual NPP distribution in the study domain.

(a) MODIS MOD17A3 annual NPP (2000- 2006 average); (b) VIC simulated annual NPP (2000-2006 average).

We chose two subdomains for evaluation of our model. First, we compared simulated methane emissions with observations reported by Glagolev et al. (2011) over the WSL (Figure 3.3). Their data are based on site observations of mire landscape methane emissions within WSL during 2007-2010. Figure 3.3 shows that our model tends to oversimulate in the middle part of the domain, but captures a general north-south emission rate gradient within WSL. Also, our emissions magnitude (1-6 gCH_4/m^2/year) tracks the observations reasonably well. As to the total

emission from the WSL area, Glagolev et al. reported a model-based estimate of 3.91±1.29 $TgCH_4$/year, as compared with our estimate of 7.12 $TgCH_4$/year. Our result is almost double the estimate of Bohn et al. (2013), because we did not use the WSL-specific soil carbon content and wetland maps (e.g. from Sheng et al. (2004)), and because we used different climate forcings. However, our estimate is within the range of estimates from inversions over the WSL, which range from 3.08 $TgCH_4$/year (Kim et al., 2011) to 9.80 $TgCH_4$/year (Schuldt, Brovkin, Kleinen, & Winderlich, 2013; Winderlich, 2012).

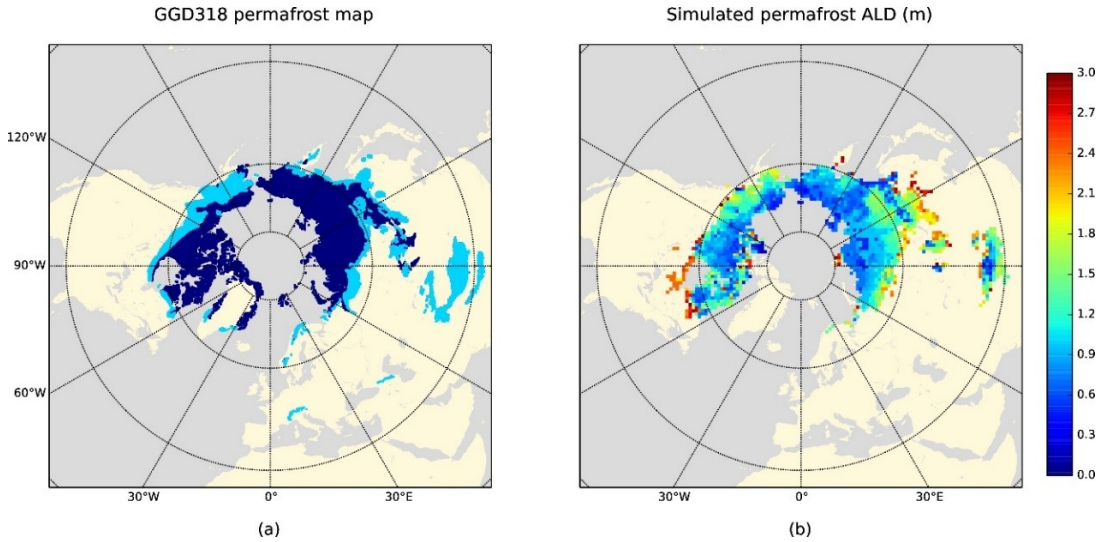

Figure 3.2: Permafrost distribution in the study domain.

(a) permafrost distribution from Circum-Arctic Map of Permafrost and Ground-Ice Conditions (GGD318 database, Brown et al. 2014). Here only continuous (permafrost extent > 90%, dark blue region) and discontinuous (extent between 50 ~ 90%, light blue region) permafrost are shown; (b) VIC simulated permafrost area with distribution of Active Layer Depth (ALD).

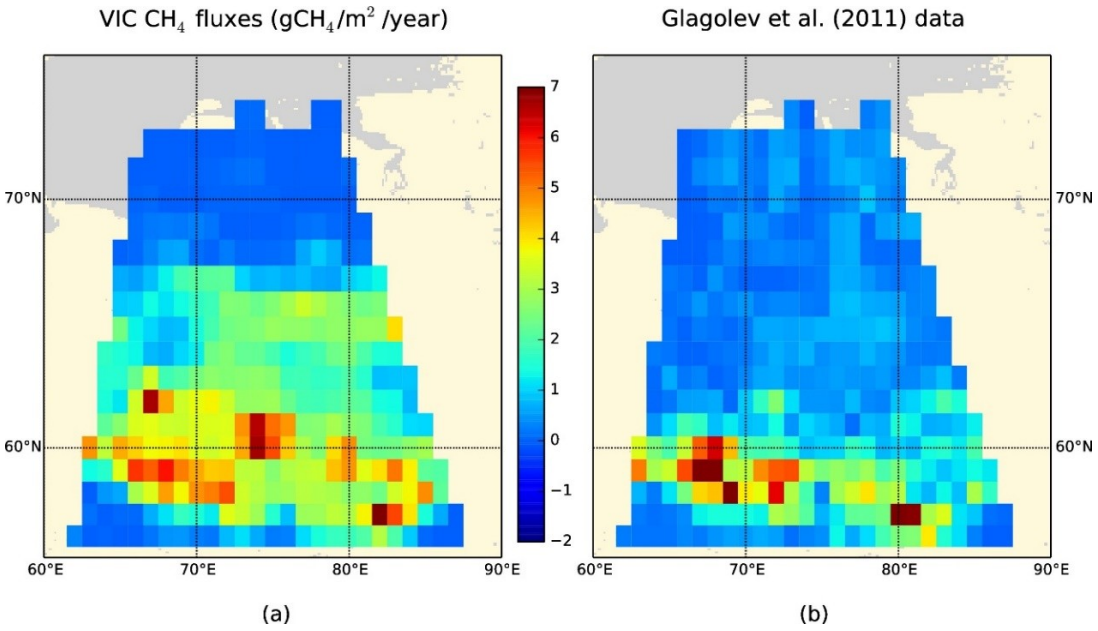

Figure 3.3: Comparison of simulated CH_4 emission rate and field campaign based data over WSL.

(a) VIC simulated fluxes; (b) field campaign data based fluxes data from Glagolev et al. (2011).

Methane emissions over HBL (here defined as the region within 50˚N - 60˚N, 96˚W - 75˚W) have been estimated by Pickett-Heaps et al. (2011) as 2.3±0.3 $TgCH_4$/year during 2004-2008. Our estimate for the same region is 3.11±0.45 $TgCH_4$/year. Although larger than the Pickett-Heaps estimate, it is almost identical to the estimate of 3.1±0.5 $TgCH_4$/year by Zhu et al. (2014). Also, for emissions in the west hemisphere part of the domain, we compared our results with those from the NCAR Model of Atmospheric Transport and Chemistry (MATCH) model (Chen & Prinn, 2006) (Figure 3.4). The MATCH study uses a 3-D chemical transport model to simulate global wetland methane emissions for the period 1996-2001. Figure 3.4 compares the total emissions from the high latitude wetland in the west hemisphere for 1996-2001. Our model

is able to represent the relatively higher emissions in 1998 and 2000. Also the total emission amount and annual variations from two studies are close.

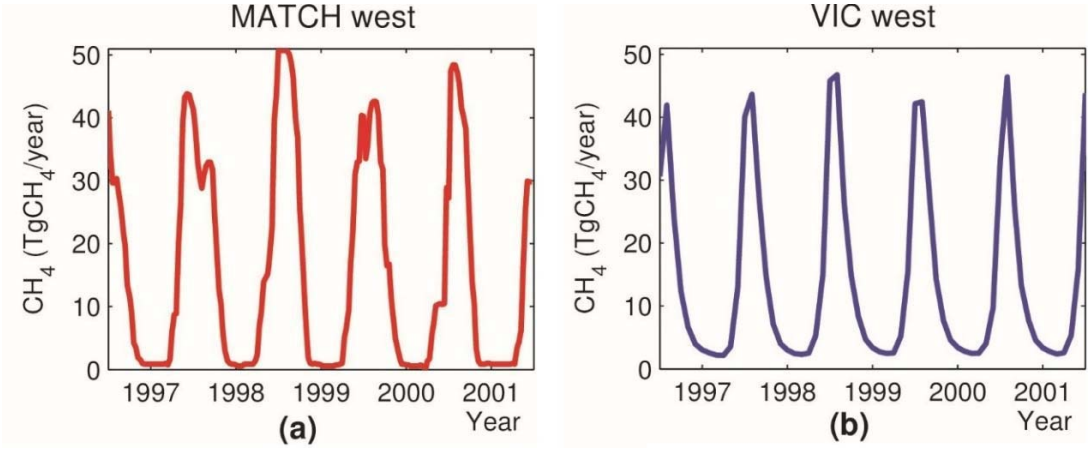

Figure 3.4: Comparison of simulated CH_4 total emission in the west hemisphere with MATCH inversion results.

(a) MATCH (Chen and Prinn, 2006) inversion results; (b) VIC simulation results. Both models show consistency in the total emission amount and pattern, also VIC captures the high emission in 1998 and 2000 relatively well.

Several studies have estimated total methane emissions in the northern wetlands (Table 3), giving a range of 20-55 $TgCH_4$/year over similar domains. Our model gives an estimate of 35.0 $TgCH_4$/year during 1960-2006. This result is within the range of estimates from studies since 1990s, and is closer to some of the more recent results, e.g. 34±13 $TgCH_4$/year estimate from Chen and Prinn (2006). The difference is well inside the uncertainty range.

Table 3: Estimates of total methane emissions over the study domain

Method	Estimate ($TgCH_4$/year)	Area	Reference	Period
VIC + Walter CH_4	35.0±6.7	Pan-Arctic wetlands	(This study)	1948-2006
VIC+TEM	38.1-55.4	Pan-Arctic area	Zhu et al. 2014	1993-2004
MATCH (inversion)	34±13	N. hemisphere high latitude wetlands	Chen and Prinn, 2006	1996-2001
Walter CH_4 model	56	Wetlands north of 45˚N	Walter et al. 2001	1982-1993
Inversion	48	Wetlands north of 45˚N	Hein et al. 1997	1983-1989
process-based model	20±13	Northern wetlands and tundra	Christensen et al. 1996	1990s
WMEM	23.3	Wetlands north of 40˚N	Cao et al. 1996	-
(literature review)	35	N. hemisphere wetlands	IPCC AR2, 1995	1980s – 1990s
(literature review)	38	Wetlands north of 45˚N	Bartlett and Harris, 1993	1980s

3.2 Sensitivity results

3.2.1 Interannual variations

Figure 3.5 shows the annual methane emissions over the domain from different climate scenarios. Panel (a) is the simulated historical emission; (b)-(f) are the methane emissions from five climate control runs. Panel (g) shows the difference between historical emissions and the climate control runs emissions, which reflect the impact of each climate factor: “TLW” is the difference between panel (a) and (b), the change of CH_4 emissions due to changes in air

temperature as well as longwave radiation; "CO_2" is the difference between panel (a) and (c), the change of CH_4 emissions due to changes in CO_2; "P" is the difference between panel (a) and (d), the change of CH4 emissions due to changes in precipitation; "SW" is the difference between panel (a) and (f), the change of CH_4 emissions due to changes in shortwave radiation. In general, climate change over the past 47 years has caused the wetland surface methane emissions to increase, except in the downward shortwave radiation control run. Downward shortwave radiation during 1960-2006 shows a decreasing trend at 95% confidence level, which is consistent with the conclusion of Wang et al. (2008). With all other inputs held constant, decreasing solar radiation leads to a smaller increasing trend in methane emissions.

Figure 3.5 shows that TLW has the greatest impact on the methane emissions, followed by [CO_2]. Saarnio et al. (1997) conclude that variations in soil temperature and carbon availability explain most of the variation in annual methane emissions. In our model, changes in soil temperature are related to changes in air temperature, while changes in soil carbon are mostly affected by changes in [CO_2] via NPP process, thus our results are consistent with this conclusion.

From each climate control run, we can also calculate a trend in simulated methane emissions, which are summarized in Table 4. Changes in temperature and longwave radiation alone are responsible for over 65% of the increasing methane emissions trend in our historical simulation. It is followed by carbon dioxide which accounts for about 15% of the total trend. The historical change in shortwave radiation is small, thus it has tiny effect on the increasing trend in historical methane emissions compared with other factors.

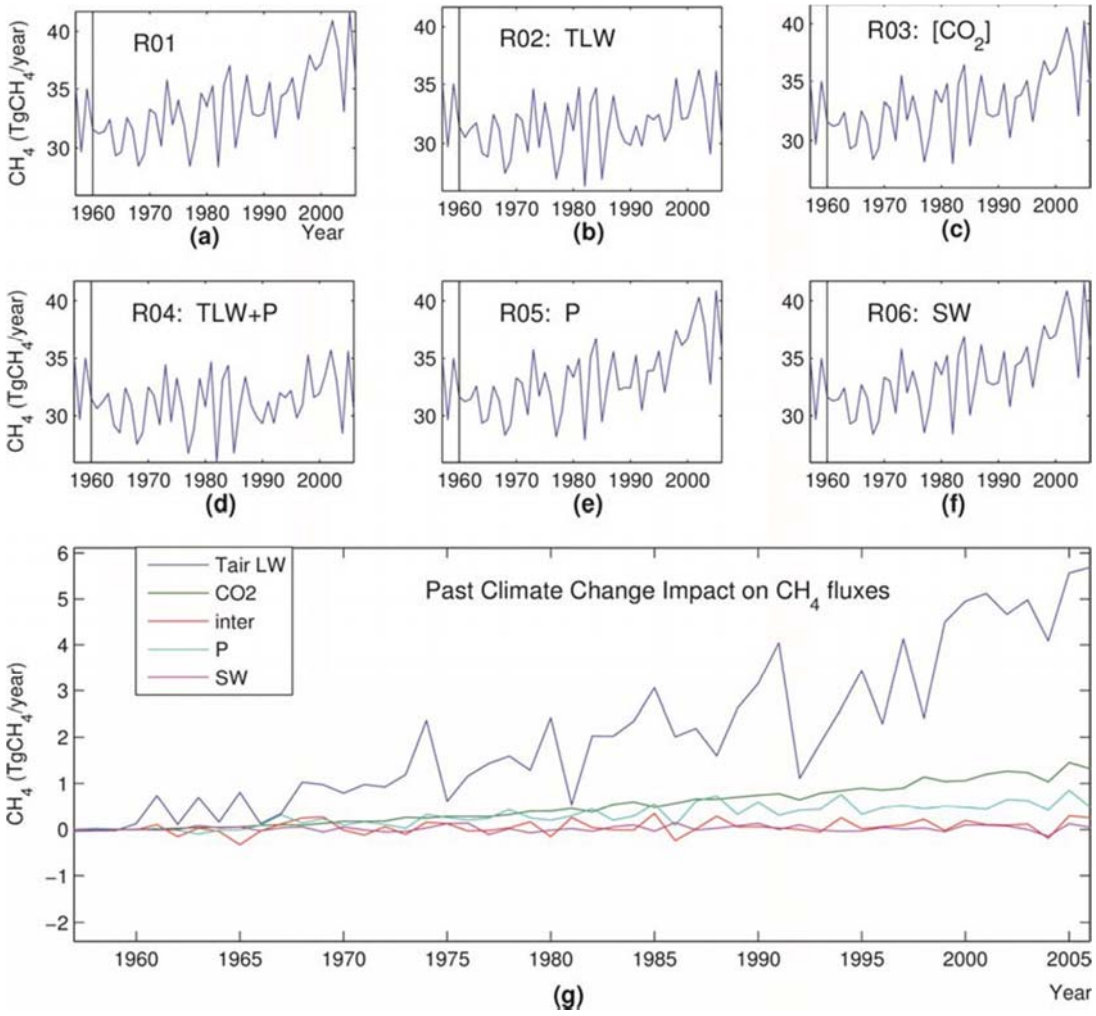

Figure 3.5: Domain averaged methane fluxes from historical simulation and climate control run with forcings detrended at 5% significance level.

(a) methane flux from the study domain under historical forcings; (b) methane flux from the domain when air temperature was held at 1960 level; (c) when CO_2 was held at 1960 level; (d) when air temperature and precipitation were held at 1960 level; (e) when precipitation was held at 1960 level; (f) when shortwave radiation was held at 1960 level; (g) the difference between historical simulation (R01) and corresponding control runs. "inter" line shows the interaction between TLW and P, and is calculated using results of R01, R02, R04 and R05.

Table 4: Trends from historical simulated and climate controlled emissions, 1960-2006

Climate scenario	Trend ($TgCH_4$/year)		95% confidence bound ($TgCH_4$/year)
historical	0.159	(100%)	(0.108, 0.210)
TLW control	0.0548	(34.5%)	(0.0055, 0.104)
TLWP control	0.044	(27.8%)	(-0.00560, 0.0938)
TLWP+CO_2 control	0.0147	(9.3%)	(-0.0338, 0.0632)
TLWP+CO_2+SW control	0.0142	(9.0%)	(-0.0340, 0.062)

3.2.2 Variations over JJA T-P space

Space-for-time substitution assumes that for spatial-temporal characteristics, the temporal distribution of a variable at a point can be approximated by the average condition for each point at different spatial locations (Pickett, 1989). Here we assume that the methane emission rates at one grid cell under different T and P conditions can be approximated by average methane emission rates at different grid cells that have various average T and P conditions. Figure 3.6a shows the distribution of multiyear average annual CH_4 emission as a function of June-July-August (JJA) air temperature (T) and precipitation (P), averaged across all wetland cells in the domain. It shows methane emission in this domain has a maximum around T for JJA of 285-295K and P for JJA of 120-200mm. It also shows that increasing P while holding T constant does not always lead to higher CH_4 emissions. This is due to the inhibition of NPP under saturated conditions in the VIC model (Bohn et al., 2013). For each grid cell, we calculated correlations between annual CH_4 emissions and the three most important climate drivers (JJA T, JJA P, and JJA CO_2) (Figure 3.6b – d). Positive correlation means that an increase in the climate driver (for instance JJA T) tends to lead to higher CH_4 emissions. In

general, high correlation of CH_4 emissions with CO_2 are everywhere, except for warm and dry conditions. At low T, correlations with T and P are essentially zero, and correlations with CO_2 are nearly one, thus CO_2 controls CH_4 emission in this climate condition. At high P and low T, there are several negative correlations with P, due to the inhibition of NPP by inundation as the water table reaches the surface. When this happens, more P tends to cause higher inundation fractions, reducing NPP and thus CH_4 production. In summary, this region is controlled by T (positively), P (negatively) and CO_2 (positively). At moderate P and moderate T, correlations with T and P are both large and positive, thus emissions are controlled by T, P and CO_2. But at moderate P and high T, correlations with P are high (nearly reaching one in places), while correlations with T are low; thus P and CO_2 control emissions here. In this region the negative influence of T on soil moisture through evapotranspiration cancels out its positive influence on metabolic rate. At low P and high T, the correlation with T becomes negative, due to drawdown of the water table as a result of increased evapotranspiration, leading to increased methane oxidation in the soil (Bohn et al., 2007). Precipitation is the dominant control under this condition. Since T and CO_2 are correlated, this is likely the reason why at the regional scale correlation with CO_2 is also negative.

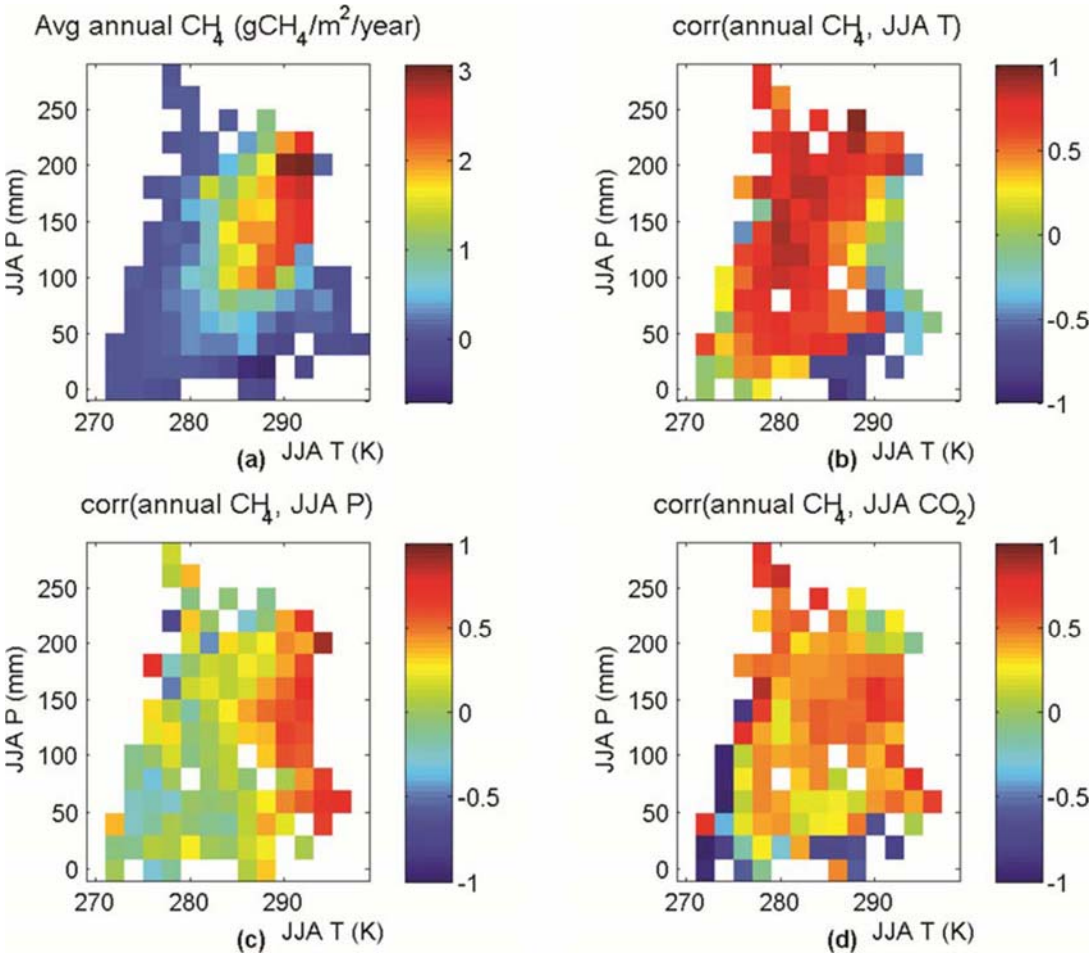

Figure 3.6: Climate relation of CH_4 emissions.

(a) the 1960-2006 average annual CH_4 emission over JJA (June-July-August) T and JJA P space; (b)-(d) correlation between 1960-2006 annual CH_4 emission and JJA drivers in the same T-P space.

3.2.3 Spatial variations in control on CH_4 emissions

Aside from a generally positive response to CO_2 everywhere, Figure 3.6 shows that the control of CH_4 emissions by JJA T and JJA P can vary widely across different climate conditions. Here we focus on the geographical distributions of sensitivities to JJA T and JJA P, to identify where each of these drivers is dominant. Figure 3.7 shows the spatial distribution of correlations

between annual CH_4 emissions with local JJA T and P. Correlations between CH_4 and JJA T are represented on a blue (positive correlation) to yellow (negative correlation) color gradient. Similarly, correlations between CH_4 and JJA T are represented on a red (positive correlation) to green (negative correlation) color gradient. Therefore blue indicates a strong positive temperature control on CH_4 emissions (T+), and this can be thought of as too cold for maximum emissions; yellow indicates a strong negative temperature (T-) control (too warm); green indicates a strong negative precipitation ("P-") control (too wet), and red indicates a strong positive precipitation ("P+") control (too dry). In general northern cells are T+ dominated (blue), due to the low air temperatures they experience most of the year. Also, a comparison with the permafrost distribution map (Figure 2.1c) shows that cells in the continuous permafrost area are mostly T+ dominated, for the same reason. As we move southward, emissions become P+ dominated (red). Southern West Siberia is relatively dry and warm, thus showing both P+ and T+ controls (orange). But in the northernmost regions of Alaska and Canada (where inundation fractions are high, see Figure 2.2b), we see predominantly P- control (green). Comparison of this figure with Figure 2.2b also shows that P+ and T- areas are correlated with smaller inundated area fractions and warmer temperatures, due to deeper water tables and greater oxidation rates.

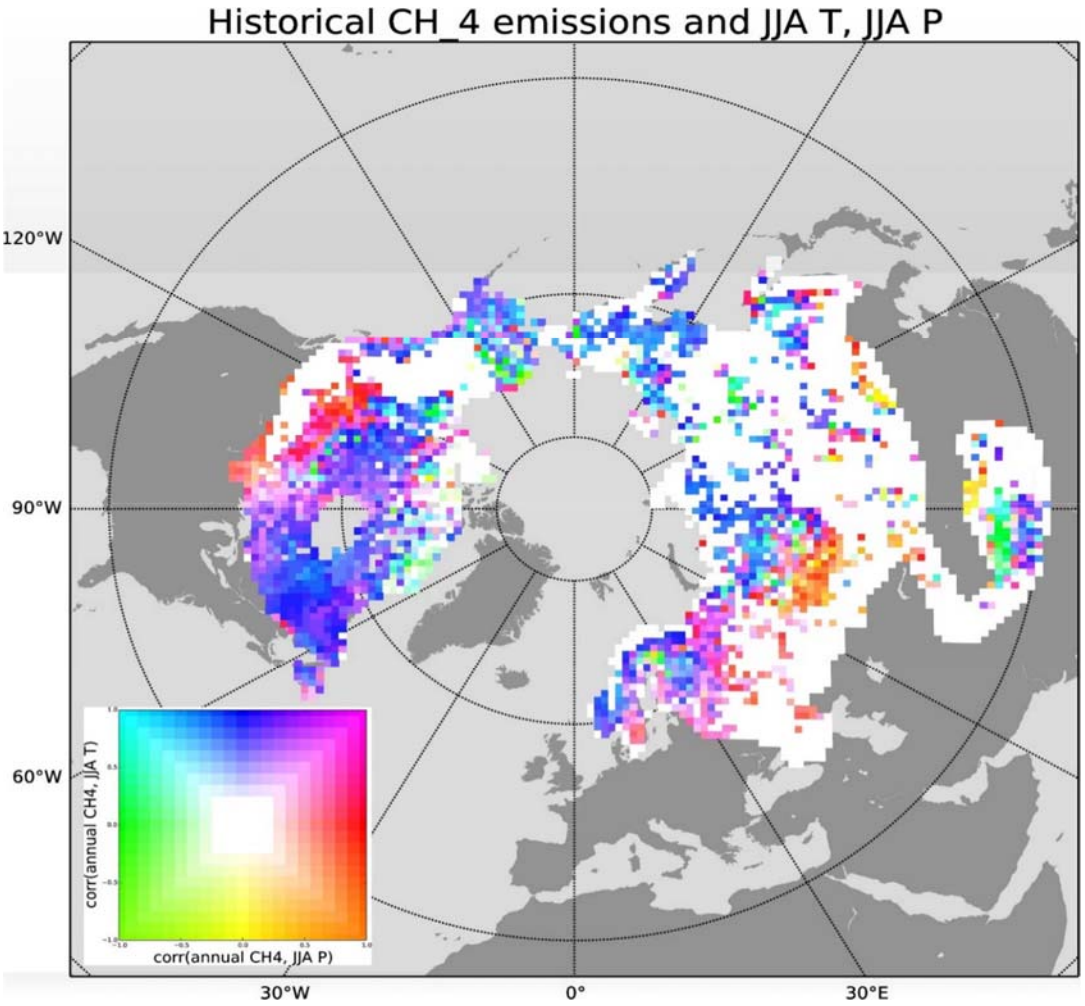

Figure 3.7: Spatial distribution of correlations between annual CH_4 emission and JJA T and JJA P.

3.2.4 Quantifying climate impacts

Figure 3.5 suggests that the interaction term is negligible when compared with air temperature or precipitation trends, so we ignore the interaction term between air temperature and precipitation. Maps of local sensitivities across the domain (Figure 3.8) display strong geographic variations. The southern WSL, south-central Canada and southern Finland have high sensitivity to all 3 drivers. These areas have high peatland fractions, which are relatively

productive (Glagolev et al., 2011; Saarnio et al., 1997), and they are outside the permafrost region (Figure 2.1c). Therefore increases in T or P would result in increases in soil temperature or moisture, and then increased CH_4 emissions. Meanwhile, these areas have high LAI, suggesting they are well vegetated. So increased CO_2 can still be utilized and result in larger NPP, thus higher CH_4 emissions. Within the permafrost area sensitivities to all three drivers are low. In those cold areas the emission rates are low (Figure 3.6a), so a slight increase in T will only lead to a small increase in emissions. Also, Figure 3.7 shows that permafrost areas are T+ dominated, so an increase in precipitation or CO_2 would only have small influence on the emission rate. Some places in southern West Siberia and southern Canada (around 120ºW) have positive sensitivity to P and negative sensitivity to T. These places are drier, so soil moisture exerts a control on methane emissions. Increased P would relieve this control, and produce more methane; whereas increased T would dry out the soil, and so the oxidation rate increases but methane production declines, resulting less methane emitted.

In general, the distributions of sensitivities are related to where each driver plays a dominant role in the biogeochemical processes. To identify the relationship between the sensitivities and various drivers (JJA precipitation, JJA air temperature, JJA inundation, permafrost condition in ALD, April-May SWE), we calculated the spatialcorrelation coefficients between them, shown in Table 5. A high correlation between CO_2 sensitivity and air temperature indicates regions that are more sensitive to [CO_2]. These generally have higher air temperatures, hence higher methane emission. A correlation of 0.34 (between CO_2 sensitivity and summer LAI, Figure 2.1b) or 0.40 (between CO_2 sensitivity and log(summer LAI)) between CO_2 sensitivity and LAI suggests that the system responds to changing [CO_2] through changing NPP. This is supported by the correlation between air temperature and LAI (0.54, which is modest). Our

vegetation mapping is static, but vegetation nonetheless responds to changes in [CO_2] via changes in NPP. In those area with higher LAI, the interannual variability of NPP (and, in turn, available carbon substrate and methane emissions) tend to be greater. Sensitivity to air temperature and precipitation are largely controlled by the general climate condition within the study domain. Air temperature sensitivity has the largest correlation with SWE. This is because higher air temperature tends to melt snow earlier and therefore moisturize the soil earlier, together with summer precipitation this makes soil stay wet for longer time. Where there is higher SWE, the soil tends to stay wet for longer time, and produce more methane. The high correlation between air temperature sensitivity and temperature itself is most likely due to the nonlinear relationship between CH_4 emission rate and soil temperature: If we categorize grid cells into two groups depending on air temperature, the average temperature sensitivity for warmer cells (mean air T > 290K) is higher than for cold cells. Given the same increase in air temperature, this nonlinearity would cause a greater increase in the CH_4 emission at places where the temperature is already high. The spatial pattern of precipitation sensitivity has no strong correlation to any specific driver. Air temperature and permafrost distributions do have some influence on the precipitation sensitivity, although neither of them is dominating. This suggests that the response to increased precipitation at high latitude wetlands is influenced by the competition between precipitation and temperature. If we categorize the grid cell into 5˚ latitude band groups, then precipitation sensitivity decreases with latitude between 50˚ and 80˚ N. A possible reason is that as we go north, air temperature decreases, thus leads to less T- constrains on the methane emission. This is also confirmed in Figure 2.3b, where P sensitivity decreases as JJA T goes down. Thus additional precipitation does not have as much effect as it does farther south. This mixed response to increases in precipitation might be from both increased soil

moisture and the inundation inhibition effect (as suggested by the fact that among the cells with less than 0.1 inundation fraction, only 33% show the negative P sensitivity; but it goes up to 41% among the cells with high inundation) on NPP, which play opposite roles on the methane emission process.

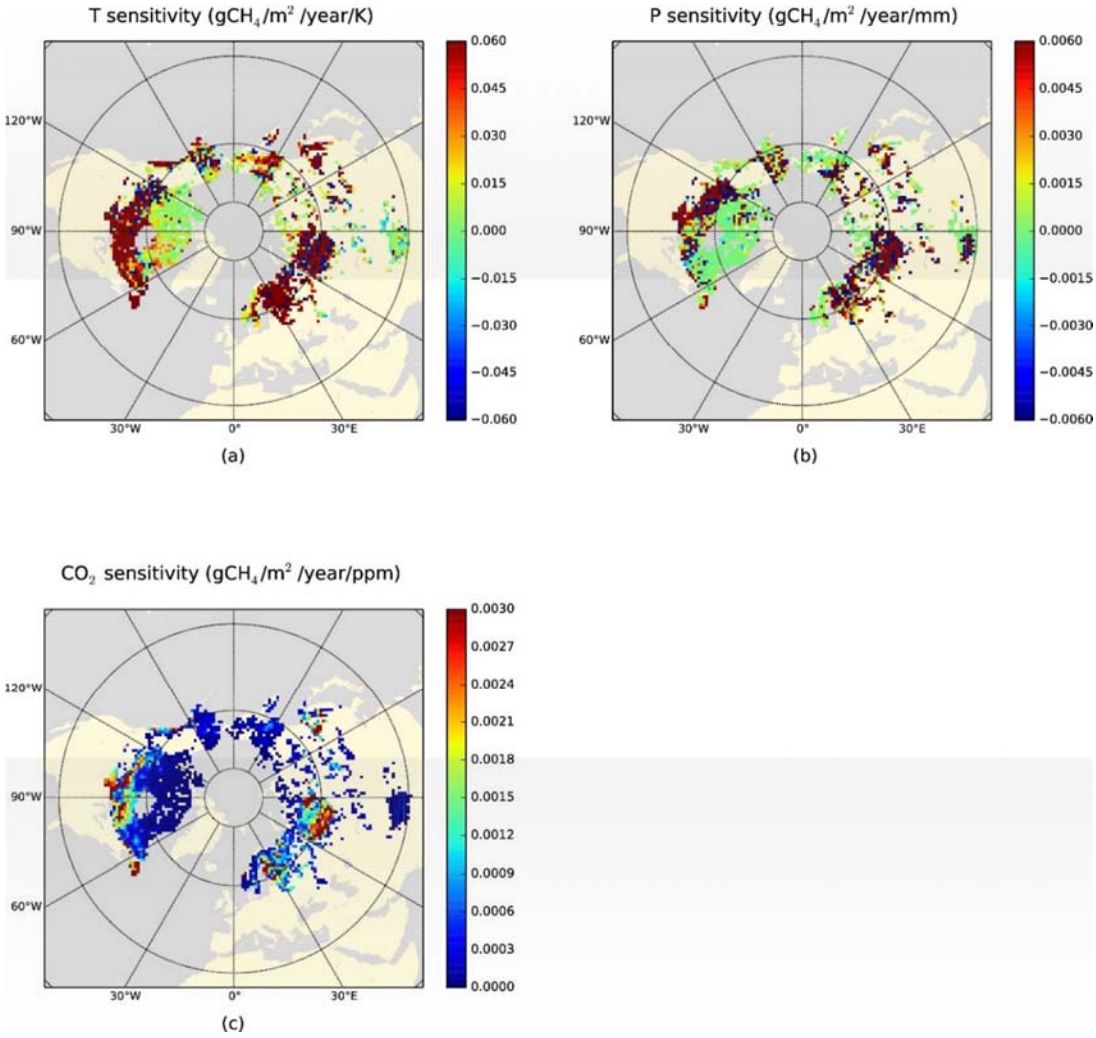

Figure 3.8: Spatial distribution of T, P and CO_2 sensitivities.

(a) air temperature sensitivities; (b) precipitation sensitivities; (c) CO_2 sensitivities.

If we plot these sensitivities in the same T-P space (Figure 2.3), they show some trends that are similar to the behavior at grid cell scale. Based on space-for-time substitution, this can be used to approximate the sensitivity of a single grid cell for different climate conditions. When it is too cold or too dry, there is little or no methane emitted, thus increasing T or P, or CO_2 will have relatively little effect under these conditions, leading to nearly zero sensitivities in the left and lower part of the three panels in Figure 2.3. In general, the sensitivities to all three factors increase with increasing T and P, due to the nonlinear dependence of methane emissions on T. The two main exceptions to this are a negative sensitivity to T at high P and low T values, due to increased oxidation; and a negative sensitivity to P at moderate T and high P values, due to NPP inhibition under saturated conditions; both of which were discussed above.

Table 5 : Spatial correlation coefficients between sensitivities and drivers.

Sens	JJA P	JJA T	JJA Ainund	SWE April + May	JJA LAI	ALD
CO_2 sens	0.3209	0.3856	0.0887	0.2951	0.3364*	0.3096
T sens	0.1827	0.1928	0.0438	0.2990	0.1735	0.181
P sens	-0.0037	-0.0088	0.0113	-0.0081	-0.0145	-0.0181

* This would be 0.3953 if we use log(CO_2 sens).

3.3 Sensitivity-based projection

One application of our sensitivity results is that it provides a basis for estimating future methane emission scenarios. As an example, we performed an experiment using CCSM4 RCP4.5 projections, and estimated wetland methane emissions for 2006-2106. We also constructed a record of repeated climate forcings and historical methane emissions during 1996-2005 as a base 100-year climate condition.

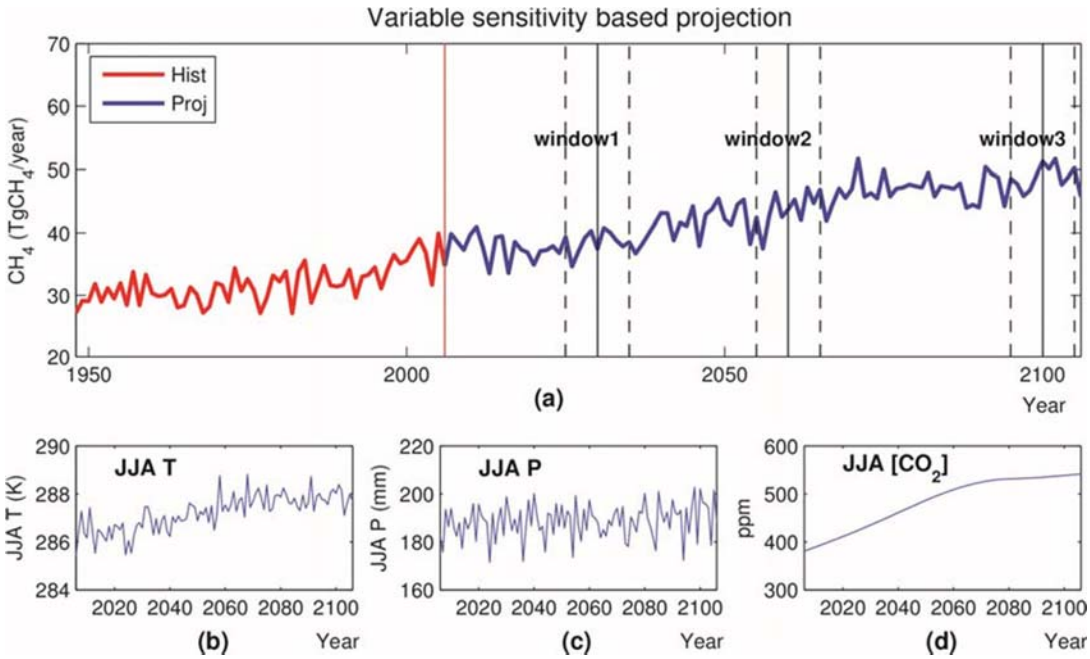

Figure 3.9: Sensitivity-based projection of methane emission from northern wetlands during 2006-2106.

(a) historical and projected annual wetland methane emissions; red line is from historical simulation, blue line is the sensitivity-based estimate of future emissions for 2006-2106; (b)-(d) climate conditions for projections. Window 1 is 2026-2035, window 2 is 2056-2065, and window 3 is 2099-2105.

Figure 3.9 shows our historical annual total methane emissions for 1948-2006, and for 2006-2106. The results from our sensitivity-based approach show that the general increasing trend during 1960-2006 continues through the end of projection at roughly the same rate of increase as in the last ~40 years.

More specifically, the projected 2060s methane emission is 44.9 $TgCH_4$/year, which is 123% of the 2000s level. At the end of the projection (2100-2106) the emission is 49.40 $TgCH_4$/year, which is 135% of the 2000s level, and 168% of the 1950s level.

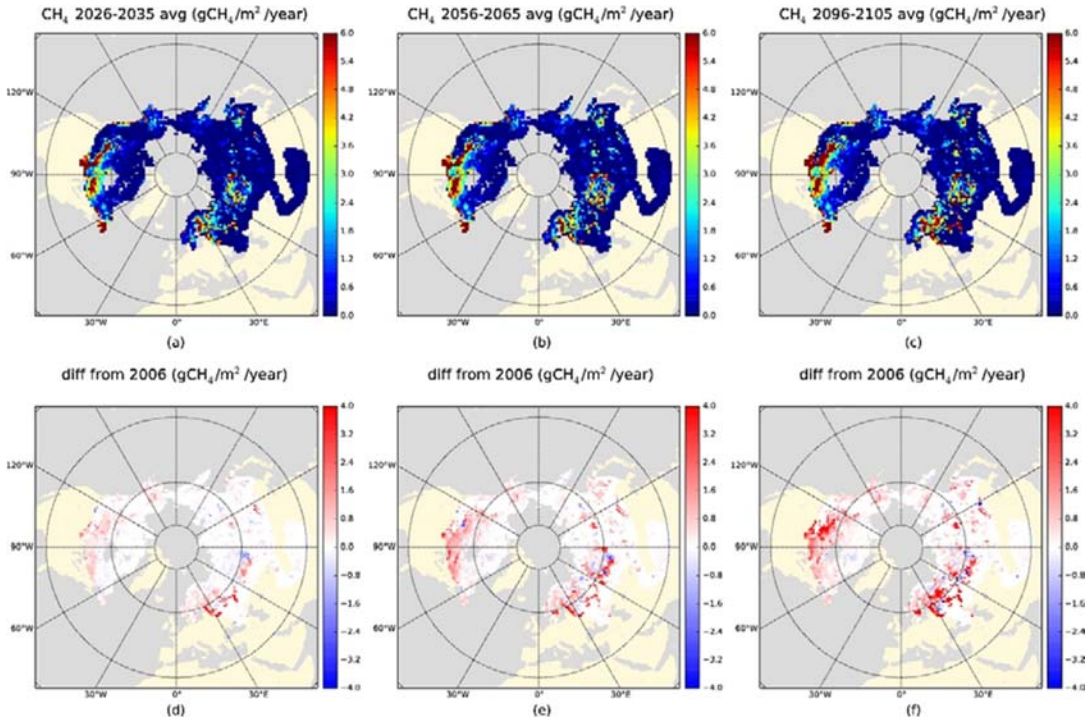

Figure 3.10: Projection of methane emission under future climate change.

(a) -(c) are sensitivity-based estimates of average annual CH_4 emissions for 3 windows in figure 3.9: 2026-2035, 2056-2065, 2096-2105; Panels (d)-(f) are differences between the estimates and 2006 historical emission.

Figure 3.10 shows the spatial distribution of estimated future emissions. Because we prescribe the wetland areas, the spatial extent of the high emissions area is similar over time. Panels (d)-(f) show the difference of emissions in these windows and emissions for 2006. There are more grid cells producing increased methane emissions (1695 cells) than those producing less methane (354 cells). The largest increases are from those grid cells with both P+ and T+ controls (purple cells in Figure 3.7).

Figure 3.11 shows the spatial distribution of correlations with JJA T and P over the three periods. We used 20-year windows to estimate these correlation coefficients. Periods 1 and 2 are the expansion of windows 1 and 2 in Figure 3.9, but because window 3 is the end of the projection, we moved this window earlier. Comparison with Figure 3.7 shows that the patterns of dominant drivers are a little different under the projected future climate: there is a trend of shifting from T+ to T- dominance. The forcings we used show an significant increase in air temperature, but not much change in precipitation (Figure 3.9b, c), thus it comes as no surprise that there will be some area shifting from current T+, P+ dominance to T-, P+ dominance. In North America, the historical T+, P+ dominated area shifts to P+ dominance by 2100, and there is a transition from historical T+, P+ to P+ dominance in 2030s, then T-, P+ in the 2060s and 2100s in southern Canada. In West Siberia, the southern T-, P+ area expands to the north, and some places in the north shift from T+, P- to T-, P+ dominance and become drier by 2100. In Northern Alaska, part of historical T+, P- dominated cells shift toward T+, P+ dominance by the end of century, suggesting that water availability has become a controlling factor on methane emissions. Also, in Finland and NW Russia, T+ historical dominance moves to P- in 2030 (i.e. it gets warmer and wetter) and then some of those cells shift to red P+ by 2100 (i.e. it gets drier). Similarly to Alaska, these areas become warmer and drier, with water availability becoming an

issue. Most of the southern cells shift from P+ dominance to T-, P+ dominance, suggesting the wetland in these area will become much drier, thus further increasing T will reduce methane emissions instead (Figure 2.3).

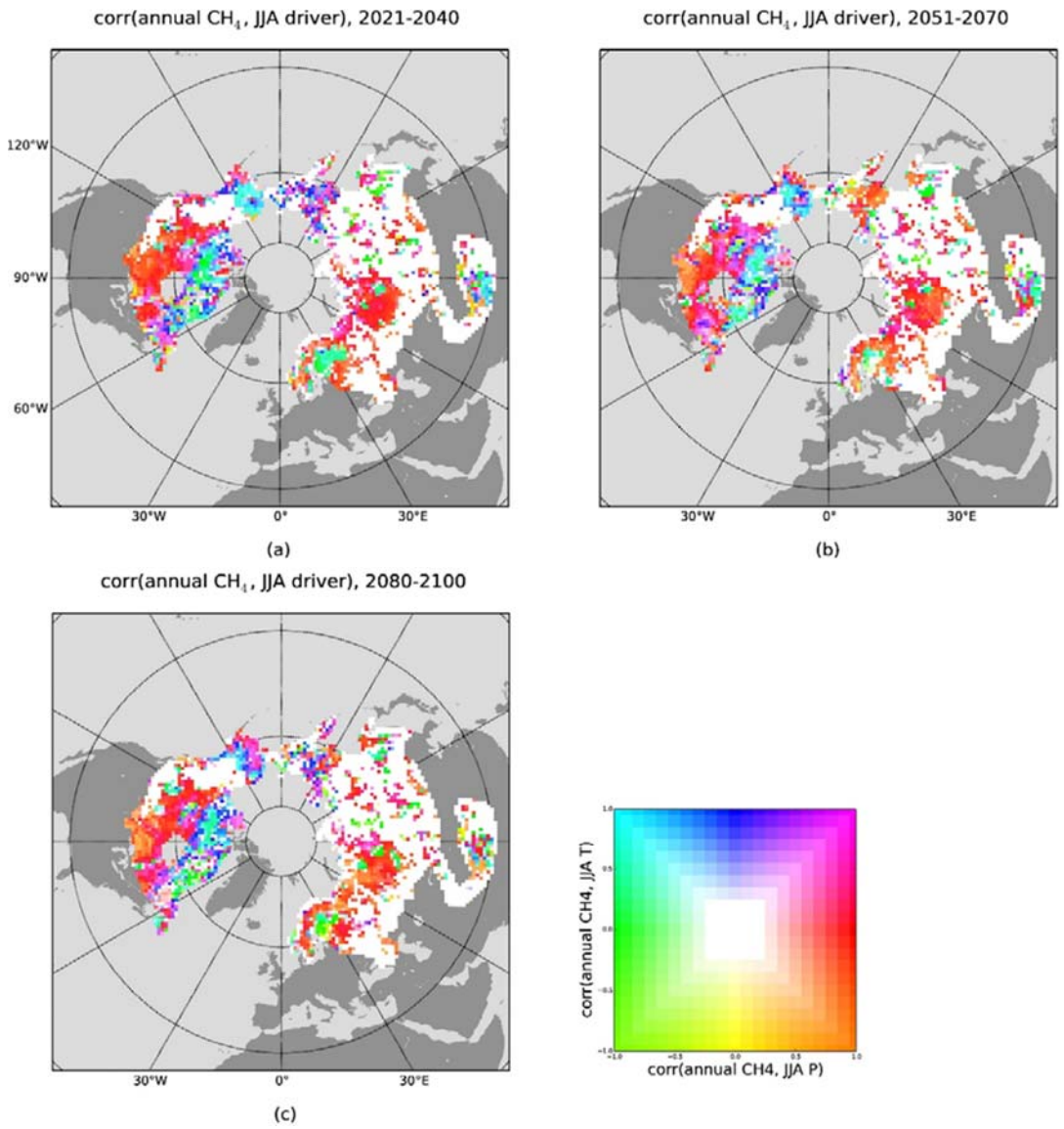

Figure 3.11: Spatial distribution of correlations between annual CH_4 emission and JJA T, JJA P from future projections.

4. Discussion

4.1 Historical behavior

Our analysis indicates that air temperature T is the dominant factor leading to changes in annual total emissions. The second most important factor was inundated area (Figure 2.2b), explaining 39% of the variance. This is consistent with Ringeval et al. (2010), who found that wetland methane emissions are correlated with variations in inundation (Ainund) and saturation (Asat) area, and variations in wetland area explained over 30% of variances in annual fluxes. In the VIC model, inundation extent depends on soil moisture conditions in the surrounding non-inundated wetlands, which in turn depend on snowmelt and summer evapotranspiration, and are thus indirectly related to precipitation and air temperature. However, since precipitation and air temperature would both affect soil temperature and moisture, it is hard to infer the changes in inundation directly from changes in climate.

The extent to which variance in inundated area is correlated to T is critical in deciding the dominant driving factor in annual emissions. Instead of separating the driving factor into T and Ainund, here we separate them as T and precipitation (P). Since T and P are available from earth system models, this is a simpler way of studying the wetland feedback to climate change. Our study period is long enough that the lag between air and soil temperature becomes less significant, and long-term trends in T should be reflected in soil temperature. From our results, precipitation does not explain much of the variance of methane emissions at an annual scale (R^2 = 0.18). Our model gives a correlation coefficient between T and Ainund of 0.47, and 0.20 between T and Asat. Thus the variation in wetland area is not significantly independent of T. It is

also this correlation that leads to the dominance of T in the variance of CH_4 emissions (R^2 = 0.49).

The dominance of T might be due to the fact that temperature is a fundamental driver of any processes in wetland production of methane. Both precipitation and air temperature strongly influence the hydrological cycle, and their influence propagates further into the biogeochemical cycle, as reflected in Table 5. However, Bohn et al. (2007) also show that these two drivers compete with each other in determining the changes of wetland methane emissions under changing climate. Figure 3.6(a) also supports this: in cold cells the CH_4 gradient is more parallel to the P gradient, while in dry cells it is more parallel to the T gradient.

However, the relatively small correlation coefficient between P and CH_4 emissions suggests that the dominance of T might be overrated. P primarily affects water table depths. If we go back to the T sensitivity maps (Figure 3.8a), they share more patterns with the LAI map in Figure 2.1b than with water table map (Figure 2.3a and b), meaning that the water table part of CH_4 response to T is less important than the metabolic part. This reflects the fact that VIC's metabolic part is stronger than its water table part. This is likely due to the way VIC was calibrated in Bohn et al. (2013). The model was calibrated to best match the Glagolev et al. (2011) map, which is based on observations almost all of which were performed on single days rather than as a multi- year timeseries. Therefore, VIC was able to better match the spatial heterogeneity of methane emissions than the temporal evolution of emissions along with changing T or water table at given grid cells.

4.2 Climate controls on methane emissions

As shown in Figure 3.7, wetland emissions in different places are controlled by different climate drivers (e.g. JJA T or JJA P). Their spatial distribution is related to local climate. Through space-for-time substitution, this can be also explained using the sensitivity in T-P space (Figure 2.3). For those areas with positive correlations with T, increasing T tends to result in more CH_4 emitted. Figure 2.3a shows that this only happens when T<290K, thus these T+ limited areas are more likely located in the north.

Similar analyses have been performed on NPP (Nemani et al., 2003) and ET (Teuling et al., 2009). Our study shares some similarity conclusions. For example, all three studies show that CH_4, NPP and ET are all T+ controlled in the south of Hudson Bay, as well as in Scandinavia. The wetlands area of southwestern Canada tend to be P+ controlled in terms of CH_4, NPP and ET. This is not surprising because NPP and ET are both tightly linked with methane production: NPP determines how much carbon can be converted to CH_4, while ET determines the soil moisture state, thus the methane production rate. In Western Siberia, the wetlands in the south are P+ and T- limited, suggesting this area is much drier than the north. NPP in this southern area is in transition from T limited to P limited, which is consistent with CH_4.

Despite their similarities, there are some differences in these spatial distributions. NPP over northern Europe and West Siberia is almost entirely limited by temperature and radiation, while CH_4 limitation includes a considerable P+ area. Figure 2.1b shows that over the regions of P+ limitation, LAI is mostly high. Trees have deeper roots than shorter vegetation, and they are able to extract water from deeper soil layers. Thus trees tend to have greater resistance to changes in P, and NPP from highly vegetated cells might not respond too much to changing P.

But CH_4 emissions drop off rapidly as the water table depth exceeds a few cm. Similarly, the P+ limited area in Western Canada in Teuling et al. (2009) is not so large as the P+ area in our study. This can also be explained by the high LAI in this area, where the moisture deficit in upper soil layers from low precipitation is partly compensated by water extracted from deeper soils. Thus only those places suffering considerable shortage of water will show up as P+ in the ET map.

4.3 Evaluation of future projections and sensitivities

Our sensitivity-based approach projects a 70% increase (relative to 1950) in methane emissions over the study domain over the next 100 years. This sensitivity-based projection follows a similar trajectory to a VIC-model-based projection, with similar end-of-century percentage increase in CH_4 emissions (Figure 4.1). Our estimate of 23% increase relative to the 2000s level by midcentury is comparable 25% increase estimated by Anisimov, 2011. For northern Eurasia wetland, we estimate the 2090s methane emission to be 21.52 $TgCH_4$/year, which is similar to the estimate of 25.08±3.66 $TgCH_4$/year by Zhu et al. (2011). The averaged trend in total emissions over Eurasia from our sensitivity-based approach is about 0.084 $TgCH_4$/year during 2006- 2106, which is about 50% higher than the estimate of 0.056±0.027 $TgCH_4$/year during 1971-2100, made by Zhu et al. (2011). This higher estimates is most likely due to lack of microbial acclimatization in our methane model.

There are some wetland processes that are not simulated in VIC model that might affect the climate controls on the methane emissions. In particular, vegetation parameters such as LAI are prescribed with a static climatology, and the potential acclimatization of soil microbial communities to changes in soil temperature are not accounted for. Studies including dynamic

vegetation phenology (Koven et al., 2011; Riley et al., 2011; Ringeval et al., 2011) generally find that wetland vegetation grows under climate change, and the increased ET tends to dry out the wetland soil. This will also reduce the inundated area, and lower water tables, thus reducing the methane emission from what it would be with constant inundation. This serves as negative feedback to climate change (termed the "wetland feedback" in Koven et al., 2011 and Ringeval et al., 2011). These effects likely explain at least part of our projected higher emissions relative to some other studies. Also, microbial acclimatization (Koven et al., 2011) reflects the adaptation of microbial community to climate change, which is presented in the model as the reference soil temperature above which methane emission happens. Accounting for microbial acclimatization would lead to a higher reference soil temperature for methanogens in the methane model, and methane emission under given temperature would be lower.

The sensitivity estimates provide a highly simplified description of wetland methane emission characteristics. They effectively lump some of the competing processes that are affected by climate change, some of which might have different effects under different climate conditions (Figure 3.6) or shifting effects as environmental conditions change, such as the inhibition effect on NPP from excess precipitation. Another major disadvantage is that even with distributed sensitivities under different climate conditions, we still have no knowledge about what will happen under climate conditions outside the historical range. Some of these disadvantages can be eliminated by involving variable sensitivities (as used here), while some can only be represented in a full simulation framework.

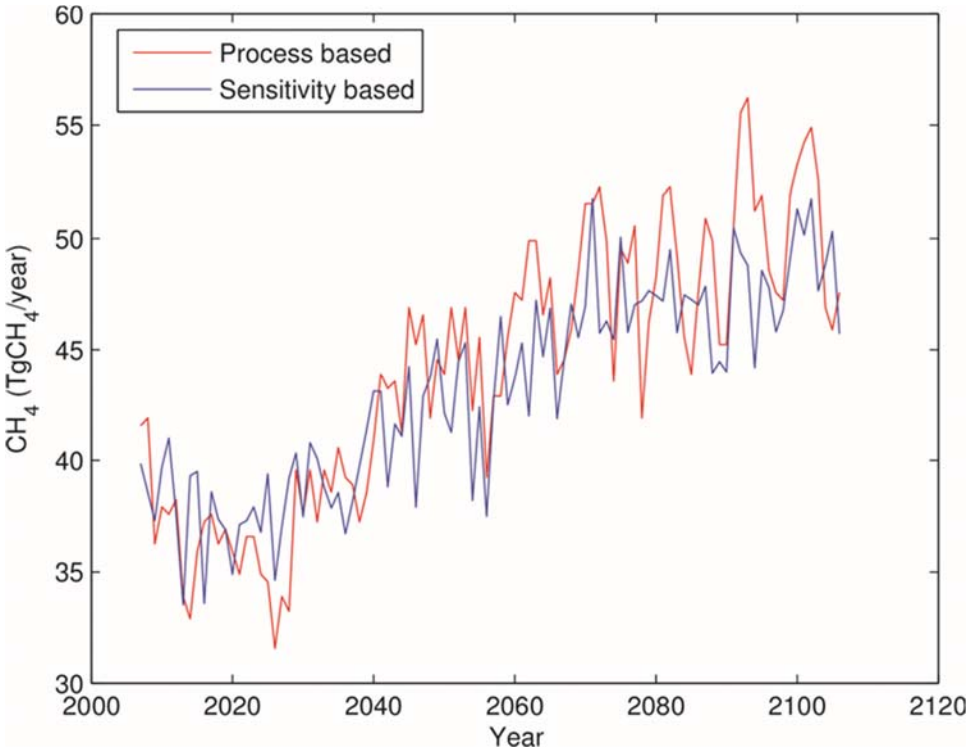

Figure 4.1: Comparison of model simulation results and sensitivity-based estimate of future methane emissions.

However, this model framework allowed us to reconstruct and investigate the historical methane emissions while avoiding these disadvantages. Linking hydrological model to methane emission model provided good description of the essential components in the wetland methane cycle (soil temperature, moisture and nutrient), and so spatial- temporal picture of the methane emissions. By running sensitivity experiments, we found that environmental control in the study domain varies greatly in space and depends on the local climate condition itself. There is a set of optimal climate conditions for methane emissions, and changes in climate conditions in different directions would result in different wetland behaviors.

5. Conclusions

We performed an historical simulation of wetland methane emissions for the global pan Arctic region. In addition, we performed five experiments that investigated the sensitivities of methane emissions to changing climate, and one future projection based on methane emission sensitivities to T, P and CO_2. Our main conclusions are:

(1) We estimate the annual methane emissions from Pan-Arctic wetlands averaged over 1960-2006 at 35.0±6.7 $TgCH_4$/year. This is slightly higher than (but within the range of) previous estimates;

(2) Past climate change has led to a substantial increase in total emitted methane, which has increased from about 29.5 $TgCH_4$/year in 1960s to about 36.5 $TgCH_4$/year in 2000s. These changes have been caused primarily by increases in air temperature and longwave radiation over much of the region, and secondarily to increases in [CO_2]. These two factors are responsible for over 84% of the projected increase. Most of the remainder is attributable to changes in shortwave radiation (decreased) and precipitation (mostly increasing);

(3) Using a sensitivity-based approach, we estimate that wetland methane emission from northern high latitude wetland will continue to increase in the coming 100 years. Under RCP4.5 climate scenario, methane emissions by mid-21st century will be about 123% of 2000s level (and 152% of the 1960s level). At the end of the century (2100s), the emissions will be about 135% of 2000s level (and 168% of the 1960s level).

(4) As future climate across the pan-Arctic becomes warmer, northern wetlands are likely to shift from the current temperature (T+) dominated state toward a precipitation (P+)

dominated state due to a lack of sufficient increase in P to compensate for higher evapotranspiration, and resultant soil drying.

REFERENCES

Anisimov, O.: Potential feedback of thawing permafrost to the global climate system through methane emission, Environmental Research Letters, 2, 045016, 10.1088/1748-9326/2/4/045016, 2007.

Bartlett, K. B. and Harriss, R. C.: Review and assessment of methane emissions from wetlands, Chemosphere, 26, 261-320, 10.1016/0045-6535(93)90427-7, 1993.

Bastviken, D., Cole, J., Pace, M. and Tranvik, L.: Methane emissions from lakes: Dependence of lake characteristics, two regional assessments, and a global estimate, Global Biogeochem. Cycles, 18, 10.1029/2004GB002238, 2004.

Bohn, T. J. and Lettenmaier, D. P.: Systematic biases in large-scale estimates of wetland methane emissions arising from water table formulations, Geophys. Res. Lett., 37, 10.1029/2010GL045450, 2010.

Bohn, T., Lettenmaier, D., Sathulur, K., Bowling, L., Podest, E., McDonald, K. and Friborg, T.: Methane emissions from western Siberian wetlands: heterogeneity and sensitivity to climate change, Environmental Research Letters, 2, 045015, 10.1088/1748-9326/2/4/045015, 2007.

Bohn, T., Podest, E., Schroeder, R., Pinto, N., McDonald, K., Glagolev, M., Filippov, I., Maksyutov, S., Heimann, M. and Lettenmaier, D.: The effects of surface moisture heterogeneity on wetland carbon fluxes in the West Siberian Lowland, Biogeosciences Discussions, 10, 6517-6562, 10.5194/bgd-10-6517-2013, 2013.

Bousquet, P., Ciais, P., Miller, J., Dlugokencky, E., Hauglustaine, D., Prigent, C., Van der Werf, G., Peylin, P., Brunke, E. and Carouge, C.: Contribution of anthropogenic and natural sources to atmospheric methane variability, Nature, 443, 439-443, 10.1038/nature05132, 2006.

Cao, M., Marshall, S. and Gregson, K.: Global carbon exchange and methane emissions from natural wetlands: Application of a process-based model, Journal of Geophysical Research: Atmospheres (1984–2012), 101, 14399-14414, 10.1029/96JD00219, 1996.

Chen, Y. and Prinn, R. G.: Estimation of atmospheric methane emissions between 1996 and 2001 using a three-dimensional global chemical transport model, Journal of Geophysical Research: Atmospheres (1984–2012), 111, 10.1029/2005JD006058, 2006.

Christensen, T. R., Ekberg, A., Ström, L., Mastepanov, M., Panikov, N., Öquist, M., Svensson, B. H., Nykänen, H., Martikainen, P. J. and Oskarsson, H.: Factors controlling large scale

variations in methane emissions from wetlands, Geophys. Res. Lett., 30, 10.1029/2002GL016848, 2003.

Christensen, T., Prentice, I., Kaplan, J., Haxeltine, A. and Sitch, S.: Methane flux from northern wetlands and tundra, Tellus B, 48, 652-661, 1996.

Crill, P. M., Bartlett, K. B., Wilson, J. O., Sebacher, D. I., Harriss, R. C., Melack, J. M., MacIntyre, S., Lesack, L. and Smith-Morrill, L.: Tropospheric methane from an Amazonian floodplain lake, Journal of Geophysical Research: Atmospheres (1984–2012), 93, 1564-1570, 10.1029/JD093iD02p01564, 1988.

DAAC, O.: MODIS subsetted land products, Collection 5, Oak Ridge National Laboratory Distributed Active Archive Center, Oak Ridge, Tennessee, 2008.

Diffenbaugh, N. S. and Giorgi, F.: Climate change hotspots in the CMIP5 global climate model ensemble, Clim. Change, 114, 813-822, 10.1007/s10584-012-0570-x, 2012.

Dutaur, L. and Verchot, L. V.: A global inventory of the soil CH_4 sink, Global Biogeochem. Cycles, 21, 10.1029/2006GB002734, 2007.

Eppinga, M. B., Rietkerk, M., Borren, W., Lapshina, E. D., Bleuten, W. and Wassen, M. J.: Regular surface patterning of peatlands: confronting theory with field data, Ecosystems, 11, 520-536, 10.1007/s10021-008-9138-z, 2008.

Fung, I., John, J., Lerner, J., Matthews, E., Prather, M., Steele, L. and Fraser, P.: Three-dimensional model synthesis of the global methane cycle, Journal of Geophysical Research: Atmospheres (1984–2012), 96, 13033-13065, 10.1029/91JD01247, 1991.

Gao, Z., Sun, B., Wang, H., Bai, L. and Wang, B.: NPP variation and its respond to precipitation change in potential extent of desertification in China during 2001-2010., in: IGARSS, 2013.

Gedney, N., Cox, P. and Huntingford, C.: Climate feedback from wetland methane emissions, Geophys. Res. Lett., 31, 10.1029/2004GL020919, 2004.

Glagolev, M., Kleptsova, I., Filippov, I., Maksyutov, S. and Machida, T.: Regional methane emission from West Siberia mire landscapes, Environmental Research Letters, 6, 045214, 10.1088/1748-9326/6/4/045214, 2011.

Gurney, K., Law, R., Rayner, P. and Denning, A.: Transcom 3 experimental protocol, Department of Atmospheric Science, Colorado State University USA, 2000.

Hein, R., Crutzen, P. J. and Heimann, M.: An inverse modeling approach to investigate the global atmospheric methane cycle, Global Biogeochem. Cycles, 11, 43-76, 10.1029/96GB03043, 1997.

Houweling, S., Kaminski, T., Dentener, F., Lelieveld, J. and Heimann, M.: Inverse modeling of methane sources and sinks using the adjoint of a global transport model, Journal of Geophysical Research: Atmospheres (1984–2012), 104, 26137-26160, 10.1029/1999JD900428, 1999.

Ito, A. and Inatomi, M.: Use of a process-based model for assessing the methane budgets of global terrestrial ecosystems and evaluation of uncertainty, Biogeosciences, 9, 759-773, 10.5194/bg-9-759-2012, 2012.

Kim, H., Maksyutov, S., Glagolev, M., Machida, T., Patra, P., Sudo, K. and Inoue, G.: Evaluation of methane emissions from West Siberian wetlands based on inverse modeling, Environmental Research Letters, 6, 035201, 10.1088/1748-9326/6/3/035201, 2011.

Lehner, B. and Döll, P.: Development and validation of a global database of lakes, reservoirs and wetlands, Journal of Hydrology, 296, 1-22, 10.1073/pnas.1103910108, 2004.

Levy, P. E., Burden, A., Cooper, M. D., Dinsmore, K. J., Drewer, J., Evans, C., Fowler, D., Gaiawyn, J., Gray, A. and Jones, S. K.: Methane emissions from soils: synthesis and analysis of a large UK data set, Global Change Biol., 18, 1657-1669, 10.1111/j.1365-2486.2011.02616.x, 2012.

Matthews, E. and Fung, I.: Methane emission from natural wetlands: Global distribution, area, and environmental characteristics of sources, Global Biogeochem. Cycles, 1, 61-86, 10.1029/GB001i001p00061, 1987.

Meirink, J. F., Bergamaschi, P. and Krol, M. C.: Four-dimensional variational data assimilation for inverse modelling of atmospheric methane emissions: method and comparison with synthesis inversion, Atmospheric chemistry and physics, 8, 6341-6353, 10.5194/acp-8-6341-2008, 2008.

Nemani, R. R., Keeling, C. D., Hashimoto, H., Jolly, W. M., Piper, S. C., Tucker, C. J., Myneni, R. B. and Running, S. W.: Climate-driven increases in global terrestrial net primary production from 1982 to 1999, Science, 300, 1560-1563, 10.1126/science.1082750, 2003.

Njoku, E.: AMSR-E/Aqua daily L3 surface soil moisture, interpretive parameters, & QC EASE-Grids V002, Natl.Snow and Ice Data Ctr., Boulder, CO, 2008.

Riley, W., Subin, Z., Lawrence, D., Swenson, S., Torn, M., Meng, L., Mahowald, N. and Hess, P.: Barriers to predicting changes in global terrestrial methane fluxes: analyses using CLM4Me, a methane biogeochemistry model integrated in CESM, Biogeosciences Discussions, 8, 1733-1807, 10.5194/bg-8-1925-2011, 2011.

Ringeval, B., Friedlingstein, P., Koven, C., Ciais, P., Noblet-Ducoudré, N. d., Decharme, B. and Cadule, P.: Climate-CH 4 feedback from wetlands and its interaction with the climate-CO 2 feedback, Biogeosciences, 8, 2137-2157, 10.5194/bg-8-2137-2011, 2011.

Ringeval, B., de Noblet-Ducoudré, N., Ciais, P., Bousquet, P., Prigent, C., Papa, F. and Rossow, W. B.: An attempt to quantify the impact of changes in wetland extent on methane emissions on the seasonal and interannual time scales, Global Biogeochem. Cycles, 24, 10.1029/2008GB003354, 2010.

Saarnio, S., Alm, J., Silvola, J., Lohila, A., Nykänen, H. and Martikainen, P. J.: Seasonal variation in CH_4 emissions and production and oxidation potentials at microsites on an oligotrophic pine fen, Oecologia, 110, 414-422, 10.1007/s004420050176, 1997.

Sabrekov, A., Runkle, B., Glagolev, M., Kleptsova, I. and Maksyutov, S.: Seasonal variability as a source of uncertainty in the West Siberian regional CH_4 flux upscaling, Environmental Research Letters, 9, 045008, 10.1088/1748-9326/9/4/045008, 2014.

Schuldt, R., Brovkin, V., Kleinen, T. and Winderlich, J.: Modelling Holocene carbon accumulation and methane emissions of boreal wetlands–an Earth system model approach, Biogeosciences, 10, 1659-1674, 10.5194/bg-10-1659-2013, 2013.

Sebacher, D. I., Harriss, R. C., Bartlett, K. B., Sebacher, S. M. and Grice, S. S.: Atmospheric methane sources: Alaskan tundra bogs, an alpine fen, and a subarctic boreal marsh, Tellus B, 38, 1-10, 10.1111/j.1600-0889.1986.tb00083.x, 1986.

Seneviratne, S. I., Corti, T., Davin, E. L., Hirschi, M., Jaeger, E. B., Lehner, I., Orlowsky, B. and Teuling, A. J.: Investigating soil moisture–climate interactions in a changing climate: A review, Earth-Sci. Rev., 99, 125-161, 10.1016/j.earscirev.2010.02.004, 2010.

Sheffield, J., Goteti, G. and Wood, E. F.: Development of a 50-year high-resolution global dataset of meteorological forcings for land surface modeling, J. Clim., 19, 3088-3111, http://dx.doi.org/10.1175/JCLI3790.1, 2006.

Solomon, S.: The physical science basis: Contribution of Working Group I to the fourth assessment report of the Intergovernmental Panel on Climate Change, Cambridge University Press, 2007.

Spahni, R., Wania, R., Neef, L., Weele, M. v., Pison, I., Bousquet, P., Frankenberg, C., Foster, P., Joos, F. and Prentice, I.: Constraining global methane emissions and uptake by ecosystems, Biogeosciences, 8, 1643-1665, 10.5194/bg-8-1643-2011, 2011.

Su, F., Adam, J. C., Trenberth, K. E. and Lettenmaier, D. P.: Evaluation of surface water fluxes of the pan-Arctic land region with a land surface model and ERA-40 reanalysis, Journal of Geophysical Research: Atmospheres (1984–2012), 111, 10.1029/2005JD006387, 2006.

Tarnocai, C., Canadell, J., Schuur, E., Kuhry, P., Mazhitova, G. and Zimov, S.: Soil organic carbon pools in the northern circumpolar permafrost region, Global Biogeochem. Cycles, 23, 10.1029/2008GB003327, 2009.

Teuling, A., Hirschi, M., Ohmura, A., Wild, M., Reichstein, M., Ciais, P., Buchmann, N., Ammann, C., Montagnani, L. and Richardson, A.: A regional perspective on trends in continental evaporation, Geophys. Res. Lett., 36, 10.1029/2008GL036584, 2009.

Walter, B. P. and Heimann, M.: A process-based, climate-sensitive model to derive methane emissions from natural wetlands: Application to five wetland sites, sensitivity to model parameters, and climate, Global Biogeochem. Cycles, 14, 745-765, 10.1029/1999GB001204, 2000.

Walter, B. P., Heimann, M. and Matthews, E.: Modeling modern methane emissions from natural wetlands: 1. Model description and results, Journal of Geophysical Research: Atmospheres (1984–2012), 106, 34189-34206, 10.1029/2001JD900165, 2001.

Walter, K. M., Smith, L. C. and Chapin, F. S.,3rd: Methane bubbling from northern lakes: present and future contributions to the global methane budget, Philos. Trans. A. Math. Phys. Eng. Sci., 365, 1657-1676, 826006M822T1417L [pii], 2007.

Winderlich, J.: Setup of a CO_2 and CH_4 measurement system in Central Siberia and modeling of its results, 2012.

Zhu, X., Zhuang, Q., Lu, X. and Song, L.: Spatial scale-dependent land–atmospheric methane exchanges in the northern high latitudes from 1993 to 2004, 10.5194/bg-11-1693-2014, 2014.

Zhu, X., Zhuang, Q., Chen, M., Sirin, A., Melillo, J., Kicklighter, D., Sokolov, A. and Song, L.: Rising methane emissions in response to climate change in Northern Eurasia during the 21st century, Environmental Research Letters, 6, 045211, 10.1088/1748-9326/6/4/045211, 2011.

Zhuang, Q., Melillo, J. M., Kicklighter, D. W., Prinn, R. G., McGuire, A. D., Steudler, P. A., Felzer, B. S. and Hu, S.: Methane fluxes between terrestrial ecosystems and the atmosphere at northern high latitudes during the past century: A retrospective analysis with a process-based biogeochemistry model, Global Biogeochem. Cycles, 18, 10.1029/2004GB002239, 2004.